Chapter 26 Handbook of Crystal Growth Vol. 3, 2nd Edition, Ed T. Kuech, Elsevier 2015, pp1057–1099 (Author-typeset version)

Self-Assembly in Semiconductor Epitaxy: From Growth Mechanisms to Device Applications

Arnab Bhattacharya
Department of Condensed Matter Physics and Materials Science,
Tata Institute of Fundamental Resaerch, Mumbai, India.
Email: arnab@tifr.res.in

Bhavtosh Bansal
Indian Institute of Science Education & Research Kolkata,
Mohanpur Campus, Nadia 741246, West Bengal, India.
Email: bhavtosh@iiserkol.ac.in

A key feature of epitaxial semiconductor crystal growth is the possibility of realizing different surface morphological features when growing one material on another. This is driven by many factors, of which the relative lattice mismatch between the materials and the nature of the resultant strain is particularly crucial. Under appropriate conditions, elastic strain relaxation can lead to spontaneous generation of coherent three-dimensional (3D) islands with relatively small size dispersion. These self-assembled islands can be embedded within a material of larger bandgap resulting in 3D quantum confinement of electrons within the island and the formation of quantum dots (QDs). In this chapter we review the strain-driven selfassembly process during semiconductor epitaxy, looking at thermodynamic and kinetic factors that influence the growth as well as specific features of QDs in various materials systems. We highlight the very fundamental correlations between structure and functionality, discuss various characterization techniques, and examine the salient features of the electronic and optical properties of QDs which make them useful for various device applications. We provide a summary of the state of the art in technological applications where the use of QD-based devices has led to improved performance and functionality. Specifically QD-based lasers, superluminescent diodes, infrared photodetectors, memories and single photon sources are discussed, with a focus on materials and growth issues.

CONTENTS

I. INTRODUCTION

New areas of research in crystal growth have opened up since the 1980s, spurred by a few key developments. Remarkable improvements in epitaxial growth techniques allowed films to be deposited with monolayer control, and developments in scanning probe microscopy enabled characterization of surfaces with atomic-scale resolution. In parallel, the use of quantum-confined structures to improve the performance of optoelectronic devices was demonstrated, especially in quantum-well lasers, and it was predicted that further improvements could be obtained by the use of three-dimensional confinement in nanosized quantum-dot (QD) structures. As device dimensions became smaller, it was realized that going beyond the limitations of traditional microfabrication techniques would require fundamentally new ideas. Electron-beam lithography patterning allows top-down fabrication of structures, with sizes in the range of tens of nanometers. However, this technique is time intensive, expensive, and often results in damage to crystallinitynone of which are conducive to device applications. The alterna-

tive is to use concepts of self-assembly a situation where structures with desirable sizes, shapes, and properties form on their own. Components of the system spontaneously aggregate themselves into stable structures. In the context of semiconductor epitaxy, the term *self-assembly* has come to specifically mean a pathway for elastic strain relaxation that leads to spontaneous generation of nanometer-sized three-dimensional (3D) islands in a bottom-up manner.[**?**]

Goldstein et al. were the first to notice the nucleation of 3D islands during the semiconductor epitaxy of ultrathin InAs/GaAs superlattices [1]. Although this was considered undesirable in the beginning, it was soon realized in three simultaneously published pioneering reports [2–4] that the 3D islands are largely dislocation-free; thus, they could be potentially important for optoelectronic device applications. Quantum confinement due to the boundary conditions imposed by the nanoscale structure profoundly affects the electronic and optical properties of these islands. Self-assembled quantum dots have thus provided a remarkable system to explore light-matter interactions at the nanoscale. The extra degree of freedom that can be controlled by the choice of materials and growth recipes has made a crucial difference in enabling new device applications. Intensive research by several groups over the past three decades to achieve uniform, high-density, and defect-free QDs has resulted in, for example, lasers with ultra-low threshold current density, new concepts for infrared detectors based on intersubband transitions, and single QD devices for quantum information processing, cryptography, and possibly quantum computation.

Self-assembled QDs synthesized using controlled growth techniques, such as molecular beam epitaxy (MBE) and metalorganic vapor-phase epitaxy (MOVPE), have been the subject of a significant amount of research in semiconductor physics and optoelectronic devices, leading to thousands of papers in the field. From understanding the basic nature of the self-assembly process to the use of QDs in advanced device structures, many different aspects of the subject have been reviewed in various books [5–15] and scholarly review articles [16–27] over the years. In this chapter, we provide an overview of the strain-driven self-assembly process, discuss the characteristics of QDs in various materials systems, examine the salient features of the electronic structure and optical transitions in QDs, then present a summary of different devices based on ensembles and single QDs.

II. SELF-ASSEMBLED QUANTUM DOTS

With growth rates that can be made as small as 0.01 monolayers per second (ML/s) [28], MBE and MOVPE allow thin-film deposition with submonolayer control. The thickness, surface reconstruction, and themorphology of a growing filmwithin the reactor can be monitored in real-time using reflection high-energy electron diffraction (RHEED) in MBE and reflection-anisotropy spectroscopy (RAS) in MOVPE. Furthermore, post-growth in-situ or ex-situ microscopy, such as scanning tunneling microscopy (STM) and atomic force microscopy (AFM), provide atomic-scale information of the surface. While this level of control has offered unprecedented technological opportunities, understanding and controlling the thin-film morphology still presents a formidable challenge. Unlike a thick liquid film on a solid surface, where equilibrium configurations can be easier reached through large-scale mass transport across the substrate, the growth and the form of the nanoscale solid surface is limited by diffusion of individual atoms. The diffusion constant can be highly anisotropic and site-specific [29]. The morphology of the growing film depends on the details of the substrate surface (its roughness, reconstruction and orientation, the nature of atomic steps), whether the substrate is planar or vicinal, the ambient growth pressure, the growth temperature, the flux of the impinging adatoms, growth interruptions, strain, alloying, and segregation. In MOVPE, the efficiency with which the undesirable metal-organic groups can be removed from the surface may be an important factor. Equilibrium configurations themselves are hard to predict because a small change in, for example, the partial pressure within the reactor can change the surface reconstruction or the diffusion bias [30], and consequently the growth mechanism. It has thus been a challenge to develop a widely applicable understanding of the self-assembled growth process in general terms and also to describe the specific role of each control variable beyond a set of empirical recipes. Here, we will mostly focus on a very general picture of heteroepitaxial growth of self-assembled semiconductor QDs, leaving out many of the important materials-specific details that one needs to worry about in practice.

A. The Stranski-Krastanov Transition

The simplest zeroth-order understanding of the thin-film growth process is obtained in analogy with the theory of liquids wetting a substrate. The competition of cohesion and adhesion forces within the film and between the film and the substrate atoms determines the contact angle and whether the film will wet the substrate. Based on the pioneering early studies of epitaxial growth by Frank and Van der Merwe [31], Volmer and Weber [32], and Stranski and Krastanov [33], Ernst Bauer in 1958 systematized the growth of epitaxial films into three categories [34]. Using the Gibbs surface energy per unit area , one can write the thermodynamic energy balance equation in terms of the surface energies Bg, Ag, and AB between substrate-gas, overlayer-gas, and substrate-overlayer, respectively [35]:

$$\gamma_{Bg} = \gamma_{Ag}\cos\psi - \gamma_{AB} + Ck_BT\ln\xi \qquad (1)$$

where ψ is the contact angle. $\xi = p/p^*$ is the degree of supersaturation given by the ratio of the reactor pressure p and the equilibrium vapor pressure of the depositing material, p^*. ξ is another thermodynamic variable that describes the driving force for the phase transition. For the condition that the contact angle $\psi > 0$ the left-hand side of Eqn 1 is less than the right-hand side. In this case the adatom-adatom interaction is larger than the substrate-adatom interaction. In this nonwetting condition, the adatoms tend to cluster together to minimize their energy, directly nucleating three-dimensional islands. This occurs when one is trying to grow dissimilar materials and when the lattice mismatch is large. This growth route is called the Volmer-Weber growth mode [35]. At the other end is the epitaxy of very similar substances, as in the case of AlGaAs on GaAs, where the magnitude of strain is less than 1.5% and the growth proceeds in a layer-by-layer manner, called the Frank-van deMerwe mode. The wetting angle is zero and the left-hand side of Eqn (26.1) is greater or equal to the right-hand side. The adatom layer completely wets the substrate and forms a continuous film, which may be mildly strained to keep to the lattice constant of the substrate. The growth in this case can proceed up to a certain critical thickness, beyond which it is energetically favorable for the film to relax the built-up strain and form misfit dislocations by partially detaching itself from the substrate. The critical thickness can be calculated by the Matthews-Blakeslee theory [36,37]. In practice, it turns out that the constraints put on by this theory are much too stringent; one can sometimes grow films of almost an order of magnitude larger critical thickness before misfit dislocations appear. For materials of a similar crystal structure (and same coordination number), the Volmer-Weber growth mode typically occurs for a lattice mistmatch of larger than approximately 7Frank-van de Merwe growth mode is observed up to around 2Although this coarse-grained energy minimization argument tells us what is thermodynamically possible, the actual mechanism of even the layer-by-layer growth is far from simple. One may visualize the layer-by-layer growth simply happening by coalescence of randomly located two-dimensional (2D) clusters of the deposited adatoms into a continuous film, but this is a very special case. In general, the growth of the initial monolayer of the deposited adatoms requires, as always for any crystal growth, formation of stable clusters of a critical size, arising from free energy minimization at the atomic scale. Step edges are typically the preferred nucleation sites. It is usually easiest for the adatoms to diffuse on planar surfaces on a given step. Going up and down the steps has an energy barrier, with the barrier for moving a step up larger than the Ehrlich- Schwoebel barrier associated with diffusion down a step [38]. This implies that the growth occurs via the propagation of steps fronts by the deposited adatoms diffusing and attaching to the nearest step edge. This mode of growth is subject to various instabilities, leading to features that are mostly considered undesirable. The result can be step- bunching, step-meandering (Bales-Zangwill instability) on vicinal surfaces [39], faceting, and the formation of mounds via the Asaro-Tiller-Grinfeld (ATG) instability in heteroepitaxy [16]. As a result of the ATG instability, the strained thin film is unstable to fluctuations on wavelength ATG, which is proportional to the inverse square of the stress f, $\lambda_{ATG} \sim f^{-1}$ [40]. The ATG instability can also yield three-dimensional clusters that are distinct from the self-assembled QDs discussed later. Strain relaxation up to the first monolayer can be also accomplished by surface reconstruction [16]. A third interesting possibility in context of Eqn (26.1) can occur during the growth of a compressively strained film with a lattice mismatch that is neither too much nor too little, between 2% and 7%. In this Stranski-Krastanov (SK) growth mode, the adatoms first completely wet the substrate, forming a strained continuous film that is a few monolayers thick. Beyond a critical thickness of this two-dimensional wetting layer, which is weakly dependent on the growth conditions, it turns out to be energetically favorable for the films surface to spontaneously transform into coherently-strained clusters on top of a thin wetting layer (WL). These self-generated three-dimensional (mostly) defect-free structures are the self-assembled quantum dots that we will focus on in this review. Examples of the systems showing the Stranski-Krastanov transition are InAs or $In_{1-x}Ga_xAs$ on GaAs, InAs on InP, and Ge on Si [16].

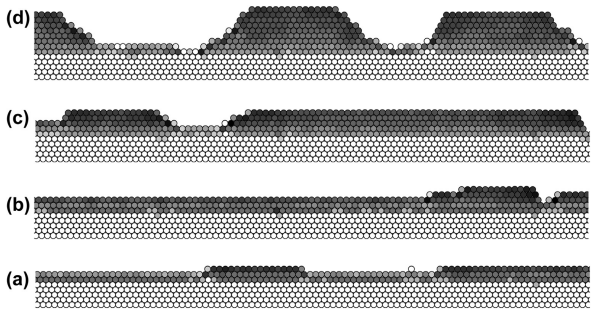

FIG. 1. Various stages of Stranski-Krastanov growth during strained-layer epitaxy captured in a simplified simulation. From bottom to top, the film morphology with increasing coverage is shown. The initial layer-by-layer growth is followed by the spontaneous appearance of the three-dimensional clusters at a critical wetting layer thickness, $WL^* = 2.3ML$. The larger islands break up and the smaller ones grow into well-defined three-dimensional clusters, with an eventual wetting layer thickness of about 1 ML. The color codes the strain: darker the particle, the larger the interatomic distance. Redrawn from original data provided courtesy M. Biehl, originally published in Chapter 4 of Ref. [15].

The Stranski-Krastanov transition can be somewhat more precisely defined to proceed via four steps following the description of Biehl et al. in Chapter 4 of Ref. [15]:

1. There is an initial two-dimensional layer-by-layer growth of the deposited adatoms, such that the film is pseudomorphically strained to fit the substrate

lattice constant.

2. This is followed by the sudden appearance of three-dimensional islands at a certain thickness of the wetting layer. This WL thickness is called the kinetic thick- ness (WL^*) and is in general larger than the thermodynamic thickness (WL_{eq}).

3. As more adatoms are deposited, the three-dimensional islands grow further. Material from the wetting layer is also incorporated into the QDs.

4. Finally, well-formed three-dimensional islands are formed on top of the wetting layer, whose final thickness, WL_{eq}, is less than the kinetic thickness WL^*.

A simulation [15] of this process of strain-driven change in surface morphology with increasing deposition thickness is shown in Figure 1. The availability of RHEED in the MBE environment provides a convenient way to monitor the evolution of the 2D to 3D transition in-situ. A comparison of the RHEED intensity, STM surface reconstruction, and AFM surface morphology at various stages for a typical case for the growth of InAs on GaAs is shown in Figure 2. The initial wetting layer thickness WL^*, on which the QD nucleation first starts, is also determined by kinetic parameters [41,42]:

$$WL^* \propto [R/D]^{\gamma}$$

where γ is between 0 and 0.5, R is the deposition rate in ML/s, and D is the diffusion constant, having an exponentially activated behavior with temperature due to the Arrhenius form of the atomic jump rate. The dependence of the WL^* on the alloy fraction, temperature, and growth flux in $InGa_{1-x}As_x$/GaAs QDs has also been systematically studied by Heyn [43]. The SK transition involving the nucleation of three-dimensional structures on the wetting layer is believed to be a first-order thermodynamic phase transition, with the island density playing the role of the order parameter. During the initial stages of growth, the island density rapidly increases and saturates with increasing coverage [28], as shown in Figure 3:

$$\rho = \rho_0(\theta - \theta_c)^{\alpha} \quad (2)$$

The parameters $\rho_)$ and θ_c in Eqn 2 are not described by the equilibrium theory and strongly depend on the factors that affect the growth kinetics, especially the growth flux and the growth temperature. This is further discussed below. Apart from these kinetic factors, more detailed work on the SK transition has revealed that although the basic picture maybe grossly correct,the actual phase diagram [44] depicting the number of islands with coverage is far more complex, with islands appearing and disappearing before the stable islands form at WL^*. Also, in the context of InAs/GaAs QDs, for example, segregation of elemental indium to the surface of the initially-flat wetting layer controls the critical point at which the transition to island growth occurs (85% indium on the growing surface) [16,45]. The QDs themselves have varying indium concentration from the base to the tip. Extending the theoretical work by Shchukin et al. [46] to include the effect of the wetting layer, Daruka and Barabasi [47] revealed further possible complexity in the equilibrium growth phase diagram with strain. Depending on the strain in the growing film, they found, apart from the usual Frank-van der Merwe and the Volmer-Weber phases, not one but two SK phases. In one of the phases, the wetting layer forms after island nucleation. It must also be emphasized that compressive strain within the 2–7% window is a necessary but not sufficient condition for Stranski-Krastanov growth. For example, even for InAs on GaAs, three-dimensional island nucleation occurs only on the (100) GaAs surface under conditions of stoichiometrically-excess arsenic. For growth on (110) and (111)A GaAs substrates, layer-by-layer growth is observed until dislocations relax the strain; on (111)B GaAs, growth of InAs occurs via the Volmer-Weber route of direct three- dimensional island nucleation [7,16].

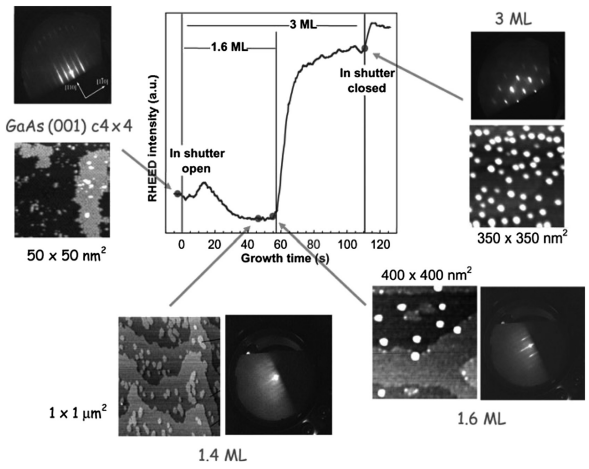

FIG. 2. Various stages in the growth of InAs/GaAs QDs monitored by RHEED intensity, STM surface reconstructions, and AFM images. The 2D to 3D transition is clearly seen between the 1.4–1.6 ML deposition stages. From Placidi et al. [27]. ©IOP Publishing 2007. Reproduced with permission.

For the growth to be properly termed as self-assembled, just the spontaneous eruption of defect-free islands is obviously not enough. Self-assembly must also imply at least some degree of regulation of the sizes and the positions of the quantum dots. Although positional order (self-organization) is generally not seen unless preferential nucleation sites are created [8], the self-assembled QDs grown via the SK route have a relatively narrow size distribution. For example, in an early review on InAs/GaAs QDs, optimal growth conditions were seen to yield fluctuations of ±5% in diameter and ±4% in height respectively, for a mean size of 30 nm and mean height of 18 nm [48].It is generally agreed that this size regulation, at least in close to equilibrium growth, is strain-induced.

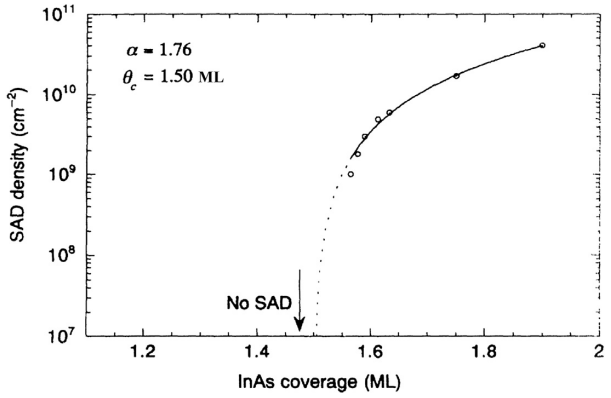

FIG. 3. Density of self-assembled quantum dots with adatom coverage. Reproduced with permission from Leonard et al. [28] ©1994 by the American Physical Society.

A lower strain is accompanied by a larger size dispersion. For example, compared to GaSb/GaAs [49]or InAs/InP [50] systems, the observed size dispersion is much narrower for InAs/GaAs QDs.

The equilibrium crystal shape is determined by Wulff construction based on the condition of minimization of surface energy. For unstrained crystals, the cluster shape is expected to be independent of size, and one may expect the sizes of islands to constantly grow at the cost of other islands (Oswald ripening) [35]. Hence, the relationship expressed in Eqn 2—which indicates that, with increasing deposition, it is the number and not so much the size that initially grows with coverageis somewhat surprising and indicates the role of stable 2D precursors. It has been proposed that the repulsive interaction between these induces a spontaneous transformation into 3D islands, which keep the same distribution [51]. The idea that size regulation and positional ordering may occur due the elastic interaction between islands due to their strain fields during coarsening has also been proposed [52]. Although these factors may be responsible for size regulation during early- and middle-stage growth well below the saturation density, at higher densities, it could simply be the energy barrier for the formation of dislocations that limits the maximum size of islands. Unlike for unstrained clusters, the elastic energy for strained clusters obviously scales with the cluster size [53]. The strain can make the equilibrium cluster shapes size-dependent [54]. Facets can self-limit island growth kinetics, which can also narrow the size distribution [55]. Wang et al. suggested that size regulation could result due to constrained equilibrium conditions, in which the island size is determined by the coverage and density, with a strong role for the wetting layer [56].

Despite various speculations, the actual mechanisms for this size regulation are still not completely understood. As we will see below, the kinetics may actually be more important in determining the ensemble characteristics.

B. Kinetics of Growth

MBE and MOVPE are essentially nonequilibrium growth techniques. The resulting structures are often metastable, sometimes quite far from equilibrium. The success in producing mismatched GaAsN alloys well into the miscibility gap [57] and the growth of defect-free SiGe [58] well beyond the critical thickness are examples where this nonequilibrium nature has found important applications. For the growth of QDs, an equilibrium configuration would imply that no change is observed during a growth interruption and the evolution of growing clusters can be reversed. This has been possible to observe only under very special circumstances [59].

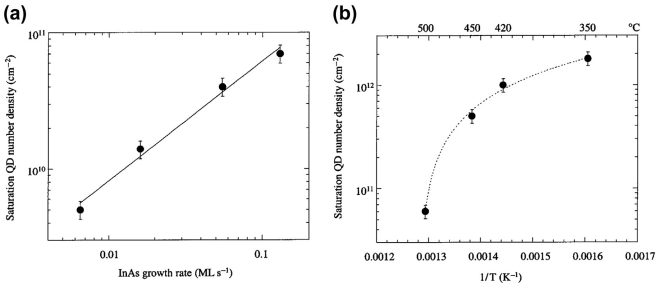

FIG. 4. Dependence of the saturation island density as (a) function of growth rate at fixed temperature (500 ^{o}C), and (b) function of temperature at fixed growth rate (0.13 ML/s). Reproduced with permission from Krzyzewski et al. [64] ©2002 by the American Physical Society.

For the specific case of InAs on GaAs, it has been possible to grow QDs with densities varying between 10^8 to almost 10^{11} cmm^{-2} for a similar amount of deposited material. The simplistic thermodynamic arguments given earlier tell us nothing about the parameters ρ_0 and θ_c in Eqn 2. This is because of the importance of transport processes in the formation of the QD ensemble. Under MBE growth conditions of ultralow reactor pressure and Knudsen cell temperatures much larger than the substrate temperature (between 450 and 550^o C for InAs/GaAs QDs), the degree of supersaturation in Eqn 1 is large. This leads to a very large driving force for crystal growth, with the chemical potential $k_BT \ln \xi$ of the order of an electron volt, comparable to the binding energy per atom on the surface. This makes the desorption of an atom extremely unlikely. Once on the substrate surface, the adsorbate atoms can then only diffuse locally on the surface until they find a suitable low-energy site or until they get covered (bound) by other impinging atoms [39]. The observed density, which depends on the average distance between islands, is thus influenced by the interplay between deposition rate and diffusion rate [60,61]. A larger adatom deposition flux leads to a larger density of QDs; increasing the temperature decreases their density as diffusion becomes more efficient. A higher temperature will also decrease the island density due to the

ease of the adatom detachment from sites of local energy minima. Parenthetically, we mention that there have also been reports of liquid-phase epitaxy of SiGe QDs, where the thermodynamic driving force for growth is likely to be at least an order of magnitude smaller and closer to equilibrium [62].

Based on these kinetic arguments, the saturation island density ρ_0 in Eqn 2 is expected to be [63,64]:

$$\rho_0 \propto R^{(i/i+2.5)} \exp\left(\frac{E_a}{k_B T}\right)$$

where i is the size of the critical nucleus, R is the deposition rate, E_a is the activation energy for diffusion, $Ea = (Ei - iE_d)/(i + 2.5)$, and E_d is the diffusion energy. From a study of InAs QDs the dependence of the saturation island density as a function of growth rate at fixed temperature and as a function of temperature at fixed growth rate are shown in Figure 26.4(a) and (b) respectively [64]. It is expected that for the other growth variables kept fixed, the island density should only depend on the ratio of the deposition flux and the diffusion rate (growth temperature); an increase in one can be compensated by a decrease in the other [60,65].

Variation of the density with temperature and growth flux is a near-universal feature observed for all systems. This simple argument, inspired by the 2Dmonolayer deposition models [66], can also be reproduced within self-consistent rate equations for average behavior, assuming atomic desorption, diffusion, attachment, and detachment processes [61]. Interestingly, there have also been attempts to understand the QD size dispersion along similar lines. Based on theoretical models for submonolayer thin-film deposition that are supported by Monte Carlo simulations [67–69], a scaling hypothesis has been proposed, in which the (monolayer) island size distribution is just a function of the average size $\langle s \rangle$:

$$N_i\left(\frac{s}{\langle s \rangle}\right) = \frac{\Theta}{\langle s \rangle^2} f_i\left(\frac{s}{\langle s \rangle}\right)$$

This implies that the island size distribution is simply

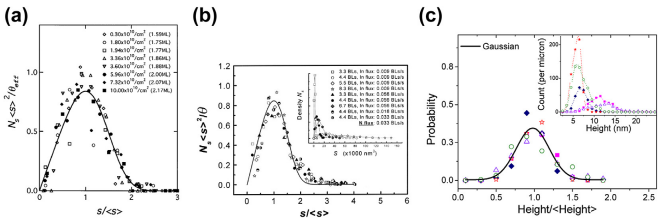

FIG. 5. Island size scaling in three quantum dot systems. (a) InAs/GaAs. (From Ebiko et al. [72].) (b) InN/GaN. (From Cao et al. [73].) Reproduced with permission. (c) InAs/InP, where it is seen that not just the QD volumes but even the heights roughly collapse to a unique probability distribution, if plotted in units of average height. (From Bansal et al. [60].)

given by a universal scaling function $f_i\left(\frac{s}{\langle s \rangle}\right)$, which is independent of coverage, temperature, and aggregation. The function $f_i\left(\frac{s}{\langle s \rangle}\right)$ has an analytical form that depends only on the size i of the critically stable cluster [70]. Quite surprisingly, this scaling was found to be valid not only for InAs/GaAs monolayer heteroepitaxy (despite the film being strained, which is not accounted for at all) [71], but also for InAs/GaAs QDs [72] at all stages of growth. However, other experiments [64] showed that it is only the later stage of growth that can be described by the universal scaling function with the critical island size, $i = 1$, giving strong evidence that later-stage growth is indeed limited by kinetics. The distribution of QD volumes collapses onto a universal curve, when plotted in units of average volume. A similar analysis has also been applied to InN/GaN [73] and InAs/InP [60] QDs. This remarkable scaling behavior in island size/height for three different materials combinations—InAs/GaAs, InN/GaN, and InAs/InP—is shown in Figure 5. Close to θ_c, on the other hand, such analysis does not always work, indicating that strain plays an important role during the initial stages of growth.

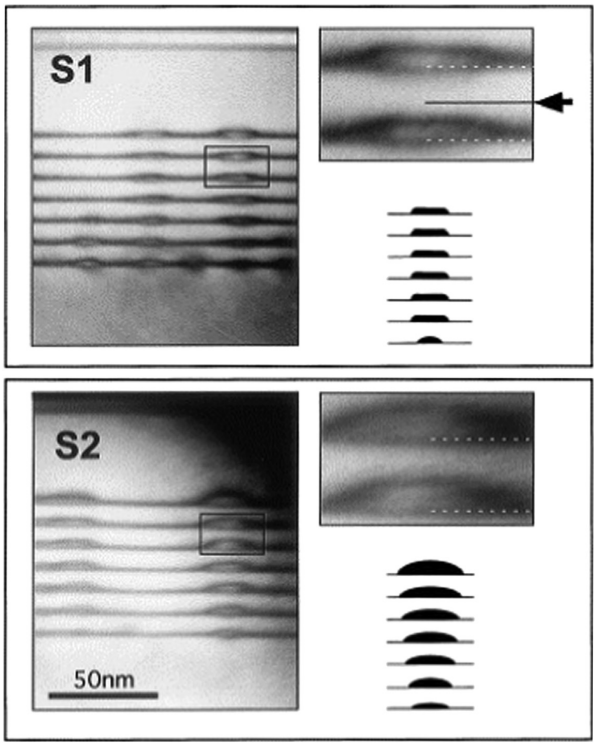

FIG. 6. FIGURE 26.6 Cross-sectional TEM images of seven-layer stacks of InAs/GaAs QDs grown with (S1) and without (S2) using the indium-flush technique. The vertical ordering of QDs is evident. For the sample S1, the dots in the multiple layers of the stack are nearly of the same size. The arrow in the high-magnification inset of sample S1 indicates the position of the indium-flush plane. Reproduced with permission from Wasilewski et al. [79] ©1999 Elsevier.

Within this general framework of scaling ideas of theoretical surface physics, the statistics of spatial correla-

tions [74] and the distribution of capture zones and excluded areas have also been studied [75] in terms of simple universal ideas with some success. The applicability of these simple ideas suggests that many of the intractably messy details of the real growth process may be not as important as they might initially seem, especially a little after the SK transition, where the growth is almost exclusively controlled by the kinetics of diffusion.

C. Correlations in Lateral and Vertical Island Positions

On a semi-infinite, flat, and isotropic surface, the position of the individual self-assembled islands that form is random. The nucleation sites for islands are influenced by the morphology of the surface (e.g., steps, reconstruction), inhomogeneous surface stress originating from subsurface features and the presence of neighboring islands. Hence, strong spatial correlations are typically seen when growing multiple layers of islands, where islands in a particular layer tend to nucleate directly above buried islands [76–78]. Further, due to the effect of the surface strain fields, the critical thickness for the onset of the SK transition in the second layer is smaller than that for the first one in many material systems. Depending on the strain anisotropy on the surface, an oblique alignment of the islands in multilayers has also been reported in a few material systems [16].

This tendency for the alignment of island locations in subsequent layers has been exploited to form vertical columns of QDs. Furthermore, the growth processes can be developed to filter out smaller dots and achieve an improved overall size uniformity. For example, the uniformity of InAs QDs in multiple layers can be greatly enhanced by the use of the indium-flush technique [79,80]. The growth of the GaAs cap layer is done in two stages. Initially, a very thin layer of GaAs is grown to partially cap the dots, following which the growth is interrupted and the substrate temperature is raised to allow the indium from the taller, uncovered features to desorb away, before growing the rest of the spacer layer. This limits the QDs in a layer to be less than a certain height and improves uniformity of multilayers. Figure 26.6 from Ref. [79] shows cross-sectional TEM images of multilayer QDs, in which the vertical stacking of dots and the improvement in size uniformity using the indium-flush techniques is evident. The redistribution of large InAs islands via interruption of the growth of the cap layer has been extensively studied in real-time [81,82] using in-situ reflectance anisotropy spectroscopy and ellipsometry, which provide useful diagnostics for optimization of the growth process.

Various simple models have been proposed to quantify the degree of the vertical correlation of island positions. A vertical pairing probability of islands that depends on the spacer thickness [76,83] is commonly used. The elastic energy release rate, defined as the change in the elastic energy of the system caused by transport of a unit volume from the wetting layer to the volume of growing island, has also been used to analyze the nucleation and correlations in positions of islands [84,85].

While the vertical correlation of islands is relatively straightforward, achieving a well-defined lateral correlation using purely self-ordering mechanisms during the growth process is more challenging. For most applications where a QD has to be accurately located within a device structure or microcavity, prepatterning of the surface is necessary to define the nucleation centers of the islands. Ref. [8] provides a very detailed review of the strategies for lateral alignment of QDs at short range using appropriate growth conditions and special substrate surfaces, as well as absolute position control over a long range using lithographic techniques.

One standard technique to achieve some degree of lateral control of island locations is via growth on step-bunched vicinal surfaces, where, under appropriate conditions, QD nucleation can be restricted to the step edge only. A periodic arrangement is hence obtained in the direction across the bunched steps, with the separation between islands determined primarily by the substrate miscut [86–88]. There is, however, no ordering in the direction along the step edge and, under high coverage conditions, the islands can merge together to form quantum wires.

III. MATERIAL SYSTEMS

The SK transition has been observed in a large number of material systems, from the relatively simple metal-on-metal growth [89] to the epitaxy of large organic molecules on metal substrates [90,91]. This section focuses on inorganic semiconductor systems, which are extensively studied due to their technological relevance and where a reasonable understanding in the growth process has been achieved by the effort of a large number of groups.

A. SiGe on Si

SiGe on Si was among the first [2,4] and the most comprehensively studied [8,16,92-94] systems. Sustained careful experiments by many groups and advances in experimental technology have allowed the growth process as function of coverage to be studied in great detail. Atomic-scale resolution of strain, alloying, and structure have pushed the understanding and control of the self-assembly process in the SiGe/Si system to a remarkable level. Ge has a lattice mismatch of 4.2% with Si, and it grows on a Si (001) surface in the SK mode with a critical coverage of 4 ML. The kinetic wetting layer thickness can be an order of magnitude larger [95].

The interest in this system arose for the following reasons: (1) Si (001) is the standard surface used for microelectronics fabrication; (2) it was realized from TEM im-

ages that the QDs that emerged were coherently strained (defect-free) [4]; and (3) it has been predicted (although not quite realized so far) that the material could in fact exhibit a direct band gap for small-sized crystallites [96], which could lead to a technological revolution in optoelectronics.

The growth of a Ge film on Si initially releases some of its strain via surface reconstruction and dimerization, with regularly missing dimers providing strain relief. On further coverage, a dense array of interlocked 105-faceted "hut clusters begin to grow.

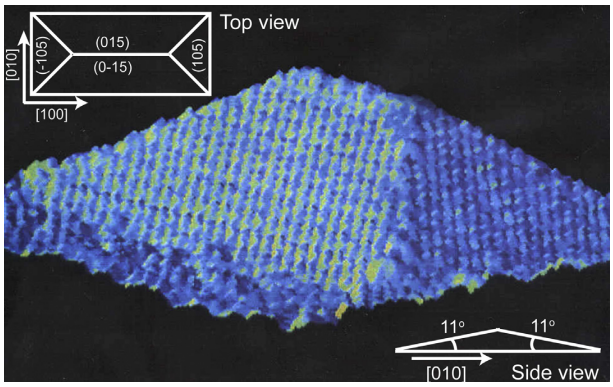

FIG. 7. STM image of $\{_{105}\}$-faceted Ge QD on Si (001) along with the schematic top and side views. The height of the nanocrystal is 2.8 nm and the base dimensions are on the order of 20 and 40 nm. This beautiful STM image of the hut cluster appeared in the pioneering work by Mo et al. [4], setting the standard for future research in this system. Redrawn from data provided courtesy M.G. Lagally, Univ. of Wisconsin-Madison and used with permission.

As shown in Figure 7, these have a rectangular base with edges in the ⟨110⟩ direction and four {105} facets, two trapezoidal and two triangular. They have a significant variation in size, with the basal area having aspect ratios between 1 and 4 and a size anywhere between 20 and 60 nm. The shapes are thought to be kinetically limited. It is not clear whether the real origin of these is a true SK transition or shallow mounds formed due to the previously discussed ATG instability.

At higher coverages, as the quantum dots are required to get bigger, structures with steeper facets and a (001) flat-top become energetically favorable because they reduce the surface area. These are classified as domes. At intermediate coverages, a bimodality in the QDs volume distribution [97,98] is observed (Figure 8), leading to the belief that these shapes represent two minimum energy configurations. The transition between huts/pyramids and domes has been proposed both as first-order transition [99] driven either by coarsening (enhancement of the feature size with coverage) [39] or elastic repulsion, and also as a kinetically-driven phenomenon with huts transferring matter to bigger domes lying nearby [100] through anomalous coarsening [101]. Here, the idea is that the energy of the cluster is size dependent and that there is a well-defined volume at which the dome energy becomes lower than the hut energy without a phase transition. This theory is sufficient to explain both the bimodality as well as the narrow size distribution [101]. The characteristic surface morphology as a function of coverage and germanium composition for the calculated phase diagrams for Ge_xSi_{1-x}/Si quantum dots is depicted in Figure 9.

Finally, as the coverage is increased further, misfit dislocations form. Under certain conditions, these dislocations themselves form an ordered network of cross-hatched patterns that may be used as nucleation sites for the growth of ordered QD arrays. Fairly regular laterally ordered QDs in a checkerboard array have been grown using the combination of surface instabilities and dislocation networks [8].

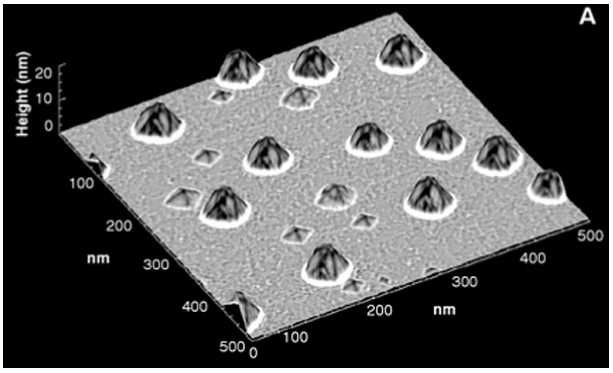

FIG. 8. STM topograph of strained Ge nanocrystals on Si (001), showing that two distinct shapes–pyramids and domes–coexist at intermediate coverage, leading to a bimodal size distribution. The figure actually shows the Laplacian of the local surface height to enhance the facets. From Medeiros-Ribeiro et al. [97] Reprinted with permission from AAAS.

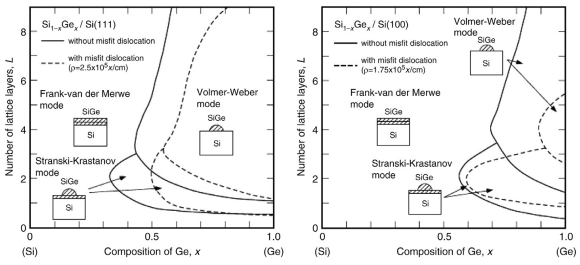

FIG. 9. Phase diagrams from free energy calculations for the growth of Ge_xSi_{1-x}/Si as a function of Ge composition (and equivalently the strain) showing the existence of various growth modes on Si(111) (left) and Si(100) (right) substrates respectively. From Berbezier et al. [94].

This discussion has ignored the chemical effects of alloying and segregation during growth. Strain can play a significant role in alloying. Both the strain and the composition of quantum dots are usually very inhomogeneous, with the regions close to the wetting layer being

both substantially strained and alloyed and the tip much less so. Intermixing also occurs during capping. If the growth is carried out at high enough temperatures, the consequent reduction in strain can drive a reverse transition from domes to pyramids to even shallow mounds [16,102].

B. III-V Systems

$In_{1-x}Ga_xAs$/GaAs: InAs/GaAs (strain 7%) is the canonical system for the study of self-assembly through the SK transition [9,14,16,19,27]. Much of the growth phenomenology discussed earlier pertains to the studies carried on this system. The type-I band alignment and the direct energy gap ensures that the radiative transitions can be observed, even at room temperature. From the characterization point of view, this makes a direct correlation between structure and the electronic states easily possible from the luminescence spectra. High radiative efficiency makes this system important for optoelectronics applications.

Therefore, apart from understanding the fundamental issues of growth, where many open questions remain (e.g., the sensitivity of the SK transition to the orientation and reconstruction of the substrate surface, dependence of the chemical composition on the growth flux), it has been imperative that the grown materials should at least have implications for practical devices that must outperform what is/was already available. Much effort in this system has been spent in achieving size uniformity and control beyond what, for example, kinetics scaling will yield. This has meant carefully optimizing the different stages of the SK growth process and tweaking all the available parameters—partial pressures, growth temperature, alloying, V/III ratio, growth flux, substrate orientations, use of surfactants, growth interruptions, alternate supply growth, punctuated growth, post-growth annealing, and using a different material for capping. Extensive literature exists on each of these. Many of the details regarding the optimization for small size dispersion are referenced in the review by Lan and Ding [103]. Other structures, such as self-assembled quantum rings, have also been grown by tweaking the growth protocol [104]. It is worth pointing out that there have been successful attempts at the creation of epitaxial islands using the Volmer-Weber growth route [105].

IV. III-NITRIDES

It has been known that the high luminescence efficiency of InGaN-based quantum-well light-emitting diodes (LEDs) and lasers arises from the spatial localization of carriers in efficient radiative potential traps, ascribed to QD-like regions spontaneously formed due to local indium compositional variations or variations in layer thickness [106–109]. Although the exact nature of the localization has been a subject of much debate, it has also motivated research in the intentional growth of nitride QDs. The lattice mismatch of 2.5% between GaN and AlN is a smaller value than that for InAs/GaAs, and the first report on the growth of GaN QDs used antisurfactant epitaxy [110]. However, QDs grown using the SK growth mode were also soon reported using both MBE and MOVPE [111,112]. Although there is much less work available than on InAs/GaAs or Si/Ge, the III-nitride material combinations offer a fascinating playground for the study of self-assembled island growth due to some of their unique properties. The III-nitrides are a material system with a large variation in band-gap difference between AlN (6.1 eV), GaN (3.4 eV), and InN (0.7 eV), which allows for efficient carrier confinement. The nitrides are also characterized by the presence of a large ($\sim$ 10 MV/cm) internal electric field along the [0001] crystal axis, arising from a combination of spontaneous and piezoelectric polarization. Because this generally has deleterious consequences for optical devices, there has been a study of nitride QDs in other nonpolar crystal directions [113-116] along the (10-10) and (11-20) planes, and also various semipolar planes [117,118]. Further even for the polar (0001) c-plane case, QDs can be growth with a Ga-terminated or N-terminated face [119,120]. Another interesting aspect is the lack of interdiffusion between a GaN QD and the AlN barrier layer during the capping process [121]. Although lot of ongoing research focuses on controlling the optical and structural properties of GaN-based QDs, an in-depth understanding is still far from being clear.

A. Other Materials Systems

Before the explosion of research in the III-nitride materials for visible-emitting devices, much effort was focused on the synthesis and characterization of II-VI quantum dots, including the demonstration of an electrically injected green CdSe QD laser [122]. Forming core-shell nanoparticles in these materials through colloidal chemistry routes is relatively simple; however, the CdSe/ZnSe combination has almost the same strain relationship as the InAs/GaAs system, thus motivating work in self-assembled island growth through epitaxial routes [123–126]. Furthermore, incorporating magnetic ions such as Mn is relatively easier in ZnMnSe and CdMnSe, and these materials have been investigated for their magneto-optical properties [127,128]. The CdSe/ZnSe QD system also exhibits a remarkable degree of Ostwald ripening on a relatively slow timescale, and it has served as a test-bed for studying the ripening and stability of self-assembled islands [129].

InP/GaInP and GaInP/GaP quantum dots have also been studied for use in the visible region. InP dots are usually deposited on a $Ga_{0.51}In_{0.49}P$ layer lattice matched to GaAs [130,131] although (Al,Ga)InP alloys with a higher bandgap are often used for better carrier

confinement [132,133]. GaInP islands on GaP substrates were also studied for visible emitters [134–136], mostly as an attempt to get around the limitation of not having any direct bandgap materials lattice-matched to the GaP—the largest bandgap "conventional" III-V substrate available. Ref. [16] provides a brief summary of the relatively less common material combinations, such as lead and erbium chalcogenide alloys, in which self-assembled island growth has also been studied.

V. STRUCTURAL CHARACTERIZATION OF SELF-ASSEMBLED STRUCTURES

From understanding the basic nature of the self-assembly process to the use of QDs in device structures, it is important that the shapes, sizes, spatial distribution, strain, and chemical composition, etc. of the self-assembled nanostructures be accurately determined. A complete structural characterization usually requires a combination of techniques, probing different physical properties at various length scales, and providing complementary information. A review of the standard techniques is provided in Ref. [16], and a detailed treatment of X-ray scattering and diffraction techniques is available in Ref. [137]. In this section, we restrict ourselves to a brief summary of the key features of various local probes, such as AFM, STM, and transmission electron microscopy (TEM) and techniques such as X-ray scattering and diffraction, optical reflectivity, and photoluminescence (PL), which usually provide average information over larger areas.

The most widely used technique to evaluate the morphology of self-assembled islands is AFM. Typical resolutions of a few nanometers in the lateral direction and about a nanometer vertically are possible, but it is important to realize that the AFM profile or image obtained is a convolution of the actual surface morphology with the shape of the AFM tip. Further, for large scan areas, the spatial resolution is often limited by the stage, not by the size of the tip. Hence, quantitative estimates should be made with care.

Although no sample preparation is required for AFM, only surface features can be imaged, making the study of buried structures such as overgrown QDs difficult. STM can be used only for conducting samples and requires an ultrahigh vacuum environment for reliable measurement. The sensitivity of the tunnel current to topography, composition, and strain, along with the atomic resolution attainable both laterally and vertically, however make it an extremely useful tool. In-situ STM has been extensively used to study the 2D to 3D transition, the development of growing facets, and shape asymmetry of QDs. Cross-sectional STM has been used to analyze buried islands, because strain relaxation at the cleaved facet leads to a height variation of the island regions, and hence change in the tunnel current. Furthermore, the elemental sensitivity of the tunnel current along with the measurement of local atom positions provides information on the shape, composition, and strain [138–140].

Transmission electron microscopy requires the preparation of thin specimens, which is often challenging; however, it provides atomic-level spatial resolution and composition sensitivity, although very locally over typically submicron-sized areas. Cross-sectional TEM is especially useful for imaging buried QDs. Because the image obtained in TEM is essentially reconstructed from diffraction data of high-energy electrons, the image contrast depends significantly on the sample preparation, elemental composition, and strain. Hence, obtaining useful information requires appropriate image processing and analysis coupled with simulation. The use of digital analysis of lattice images (DALI) after filtering [141,142] and lattice-fringe analysis [143] allows accurate determination of the variations in unit-cell spacing and local strain. In combination with energy-filtered TEM imaging and scanning TEM (STEM), by which element-specific information not affected by the strain can be obtained, comprehensive characterization of self-assembled islands using TEM allows determination of concentration gradients within QDs, strain profiles around buried islands, correlation of island positions, etc. [144–146].

Nanostructured materials have been probed via techniques using X-rays in various scattering geometries that allow nondestructive investigation with penetration depths that can be tuned from several nanometers for surface studies to a few micrometers to study buried structures. In all methods, the intensity distribution of scattered or diffracted beams in the reciprocal space is recorded, and appropriate modeling and fitting procedures are necessary to realistically interpret the experimental data. The beam diameters typically cover a few hundred micrometers to several millimeters, thus allowing sampling over a very large number of islands and good measurements of average values.

Grazing-incidence small-angle X-ray scattering and X-ray reflectivity are not sensitive to the crystalline structure of the samples. In these methods, contrast arises due to differences in the index of refraction. Thus, these techniques have been exploited to determine investigation of the island shape, correlation of island positions, and interface roughness of self-assembled islands [83,147–149]. On the other hand, in X-ray diffraction, the main contrast arises due to strain. Typically, reciprocal-space maps recorded around symmetric and asymmetric Bragg reflections are analyzed to extract the strain in the islands and the surrounding layers, as well as evidence of intermixing and change in shape of the islands [150]. To improve surface sensitivity, grazing-incidence diffraction is often used, which due to the low penetration depth is sensitive primarily to the in-plane lattice parameter, not to lattice parameters and strains in the growth direction. The technique of isostrain scattering [151,152], combining in-plane diffraction and vertical reflection at grazing incidence, enables the virtual decomposition of a 3D island into slices at different heights and allows a map of

composition and strain to be obtained. In combination with techniques such as extended X-ray absorption fine structure, additional information on the local chemical environment can be also be obtained [153–155].

Nondestructive optical techniques are routinely used for in-situ monitoring of epitaxial growth in MBE and MOVPE environments, especially with the widespread availability of sensors for multiwavelength reflectivity, reflection-anisotropy spectroscopy, and curvature measurements. The changes in overall stress [156], intensity of scattered light [157], and/or surface reconstruction [82,158] at the 2D-3D transition with increasing coverage, or on shape transitions, provide qualitative information useful for monitoring the growth process and real-time control [159].

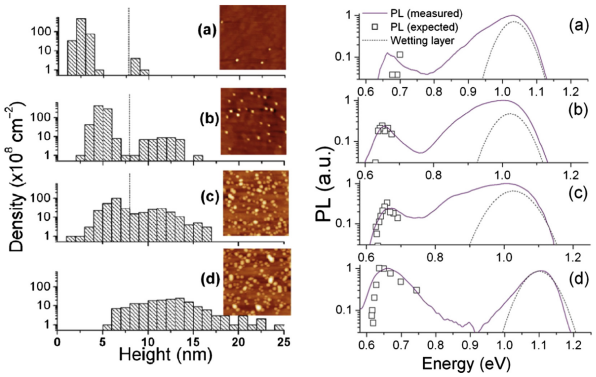

FIG. 10. Correlation of QD surface morphology with photoluminescence spectra. Left: AFM topographs and histograms of island heights (plotted on a log scale) at coverages of (a) 4.5 ML, (b) 6.5 ML, (c) 9 ML, and (d) 14.5 ML for MOVPE-grown InAs/InP. Right: PL spectra measured from samples grown under similar conditions, but with an InP overlayer. Using QD-size-dependent transition energies, the PL spectra corresponding to the larger dots can be reconstructed (shown as squares) from the height histograms without any fitting parameter. PL from the wetting layer (dotted line) appears at $1.02 - 1.03$ eV in (a)-(c) and shifts to 1.10 eV for (d), indicating that the wetting layer thins down to an equilibrium thickness at the later stage of growth. Redrawn from the authors' original data, adapted from Bansal et al. [50].

As ex-situ tools, PL and electroluminescence (EL) spectroscopy are the standard probes to evaluate the optical quality of self-assembled islands. Conventional PL spectroscopy typically has an excitation laser spot size of $>\sim 100\mu$m, thus exciting a large ensemble of $>\sim 10^6$ QDs. Although the PL spectra are hence inhomogeneously broadened due to the unavoidable dispersion in QD sizes and composition, luminescence from ensembles is still a very useful technique, with the emission linewidth providing some measure of island uniformity. At low excitation power, typically only emission from the ground state is observed, and absorption spectra are required to see the higher energy levels. However, the absorbance of a single layer of QDs is very low and difficult to measure, and related techniques such as photocurrent spectroscopy, PL excitation, and modulation spectroscopic techniques, such as photoreflectance, electroreflectance, or surface photovoltage spectroscopy, are experimentally more convenient [19]. Single QD spectroscopy is performed either on specially patterned structures having single dots or on samples with very low island density, or by masking the surface and opening up a submicron-aperture through which the luminescence can be measured. Correlating the structural information (e.g., from AFM) with the electronic and optical properties (e.g., from PL) often provides useful, albeit qualitative, information on the growth process and the development of islands. Of course, AFM images are typically obtained on uncapped QDs and cover an area of a few square micrometers, vastly different from the $\sim 1\text{mm}^2$ area sampled in PL measurements on capped samples. As an example, consider the case of MOVPE-grown InAs QDs grown on InP [50] shown in Figure 10. The left panel of Figure 10 shows a series of histograms of island height distributions inferred from 1μm AFM for samples with increasing InAs coverage. The corresponding low-temperature PL spectra measured on the overgrown samples with the InAs layer deposited under identical conditions is shown on the right. Using published ground-state energy calculations [160] for pyramidal InAs/InP QDs, the expected emission spectra from large dots are shown in Figure 10(b) as open squares. There is a remarkably good quantitative agreement (without any fitting parameter) for the expected and observed spectral features from large islands. In this particular set of experiments, the samples had a bimodal distribution of island sizes. The smaller features are much more sensitive to the capping process and As/P exchange during overgrowth and do not show a similar correlation between the AFM data and the PL.

VI. ELECTRONIC STATES AND OPTICAL PROPERTIES OF QUANTUM DOTS

The interest in self-assembled quantum dots stems from the profound difference in their electronic and optical properties in comparison with bulk materials [6,9,14,18]. As the size of the crystal is made comparable to the de Broglie wavelength of carriers, the electrons and holes begin to experience the boundary of the crystal. The three-dimensional localization of the carrier wave functions within the quantum dot, due to corresponding momentum uncertainty, increases the minimum allowed carrier kinetic energy, thereby effectively increasing the energy gap of the material. Quantum confinement thus offers an extra degree of freedom (like alloying and strain during heteroepitaxy) to control, at the most fundamental level, the energy gap of the resulting nanocrystal over a wide range. For example, in InAs QDs grown on GaAs, the fundamental energy gap can be enhanced from its bulk value of 0.35 eV to close to 1 eV. Confinement of charge carriers also leads to a

qualitative change in the structure of the electron and hole density of states. The energy levels now appear discretely, well-separated from each other as in atoms. This is the defining characteristic of all types of quantum dots, whether lithographically made [161], colloidal [162,163], or self-assembled. These changes in the electronic density of states, the energy levels, and the carrier distribution functions on account of one-dimensional (quantum wells), two-dimensional (quantum wires), and three-dimensional (QDs) confinement are depicted by the schematics in Figure 11.

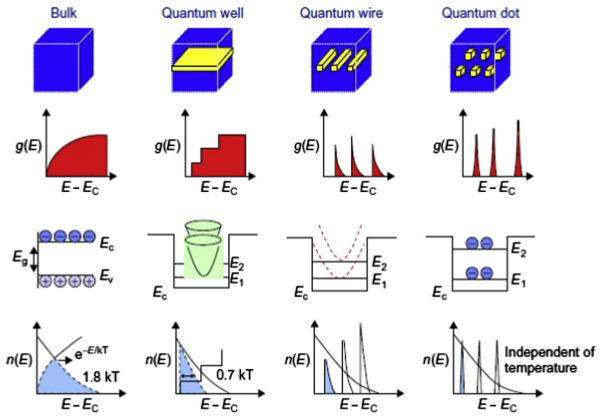

FIG. 11. Schematic of the change in the electronic properties of semiconductors with dimensionality as one goes from bulk (3D) to quantum well (2D), quantum wire (1D), and finally QD (0D). The character of the density of states significantly changes and the electronic energy levels evolve from bands (3D) to subbands (2D and 1D) to atomic-shell-like levels in QDs. The bottom figures show the thermal spread of the electronic distribution function in the corresponding cases. The fact that the carrier distribution is more or less independent of temperature in QDs gives thermal stability to the operational characteristics of devices, an aspect of great technological significance. From Barve et al. [23].

A typical self-assembled quantum dot comprises of approximately $1 \times 10^4 - 5 \times 10^4$ atoms; therefore, no two QDs are ever likely to be identical. Moreover, unlike atoms, there are no fundamental symmetries. The devil is in the details, which on the one hand make good quantitative modeling of the experimental observations very difficult, while on the other offer a rich playground for novel application ideas.

The first and the most important detail is the material combination used during heteroepitaxy. It is a happy coincidence that, between two similar materials, the one with the larger lattice constant will also typically have a smaller energy gap [164]. Therefore, the necessary condition for Stranski-Krastanov growth (compressive strain) is also often accompanied by the material forming the QD having a smaller energy gap than the substrate. Quantum dots are almost always capped with the same material forming the substrate. Capping also minimizes dangling bonds and surface states on a free surface, which typically provides efficient routes for nonradiative recombination and quench radiative emission. For such embedded QDs, the boundary conditions on the carrier wave functions are now determined by the relative band offsets at the heterointerface [165]. Materials with type-I band alignment are most studied. For the same material forming the QD (e.g., InAs) choice of a different substrate (e.g., InP instead of GaAs) can lead to very different energy gaps. The band offset can be sensitive to the details of the QD structure, its shape, strain, and composition and needs to be experimentally established for newer materials [166].

After the size, nature, and extent of band offsets, the other important parameter that dictates electronic properties is the shape of quantum dots. Although solution-grown nanocrystalline QDs are well-approximated as spherical [162], we have seen that self-assembled QDs can exist in a variety of shapes and continuous range of sizes and aspect ratios. Typical QDs are much wider than they are high. Heights typically range from 3 to 15 nm and the base diameters between 20 and 60 nm. Therefore, the primary confinement results from their height. Furthermore, the Stranski-Krastanov grown QDs sit on a wetting layer, which implies that the electronic states within the QD are coupled to the states of a thin quantum well [167]. The strain relaxation within the QDs is partial and inhomogeneous, with capping inducing further strain. The capping can also denude the QD of some material and significantly change its shape [168]. As discussed earlier, there is a fair amount alloying and intermixing of the materials making up the QD with the substrate material. Indium in particular has a tendency to segregate [45].

Given that the basic physics of electronic states and elasticity in semiconductors (the multiband effective mass formalism or the pseudopotential theory for the band states, effect of strain, and alloying on the band structure) is relatively simple and very well understood [169], materials theorists can run very realistic numerical calculations of the energy levels and optical properties of QDs, which include in detail the exact shape, strain, and alloying. The early and much cited works by Grundmann and coworkers considered the pyramidal shape of the QDs, and the strain using the valence force field or the continuum elasticity theory. Initially a single-band effective mass theory and later an eight-band $\mathbf{k}\cdot\mathbf{p}$ theory was used to account for the electronic states [170a,170b]. There have been reasonably successful attempts to correlate the optical spectra with detailed calculations using the size, shape, strain, and composition information obtained from cross-sectional STM on the same sample [171]. However, given the size, shape, composition, and strain variation among the QDs (even on the same sample) and the sensitivity of various band parameters to these details, the meaningfulness of such an exercise is doubtful, especially for macroscopic ensemble measurements. Similarly good results can sometimes be obtained via much simpler analysis [50], such as by assuming a

parabolic confinement potential (e.g., see Chapter 2 of Ref. [11]). An accessible introduction to the computational aspects of the electronic states in QDs is given in Ref. [172], and user-friendly research-level software packages implementing sophisticated algorithms are also now freely available [173].

The discrete energy-level structure is clearly seen in electrical charging experiments using capacitance spectroscopy and also in optical measurements such as absorption, reflectance, and photoluminescence spectra [174,175]. What is typically measured in macroscopic experiments is the collective response of about 10^6 QDs over a dimension on the order of $100\,\mu$m. The measured response is thus an inhomogeneously broadened spectrum comprised of the additive response of individual levels, each homogenously broadened by a few meV. This is illustrated in Figure 12(a), where the broad emission peak measured over a macroscopic area of the sample can be seen to be actually a collection of very narrow discrete peaks from single QDs when the area from which light is collected is reduced to microscopic dimensions. Furthermore, the spectra from individual QDs can exhibit a fair amount of complexity (Figure 12(b)).

The observed linewidths are of the order of $10-30$ meV for ensembles of InAs QDs on GaAs. Other material combinations can lead to inhomogeneous linewidths in excess of 100 meV (GaSb/GaAs). Electronic coupling between QDs is only important at very high densities.

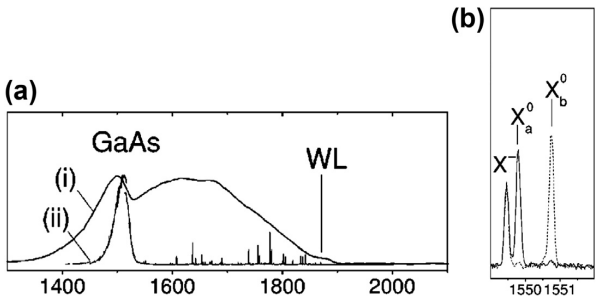

FIG. 12. (a) Ensemble PL measurement from a $InAs/Al_{0.6}Ga_{0.4}As$ QD sample (i) shows a broad peak, inhomogeneously broadened due to the additive contribution of the emission from a large number of QDs. PL recorded from a small region of the sample (ii) shows sharp discrete lines corresponding to the emission from individual dots, each having a slightly different ground-state energy. (b) Individual QD emission can be polarized. The peaks X_a^0 and X_b^0, seen for two different linear polarizations, correspond to two different excitonic transitions. X^-, the charged exciton transition, is insensitive to linear polarization. Reproduced with permission from Finley et al. Ref. [175] ©2002 by the American Physical Society.

Quantum dots comprised of direct gap semiconductors are very good light emitters. This is because the spatial confinement of electrons and holes results in a larger wave function overlap and consequently enhanced oscillator strength. Further, the localization of carriers also leads to a relative insensitivity of the emission strength with increase in temperature. While the luminescence from bulk and quantum wells is seen to rapidly quench by approximately 50 K, emission from QDs is seen to persist up to room temperature. Since the pioneering experiments [176,177] in the mid-1990s, much experimental effort has gone into single-quantum-dot spectroscopy, both electrical and optical [8]. In the category of electrical experiments, scanning tunneling microscopy has been used to map the electron and hole densities associated with individual orbitals within the single dot [178].

Optical spectroscopy of quantum dots, both single and in ensembles, has become a field in itself. Broadly, the focus has been on the nature of exciton states, interdot carrier transfer processes, and the physics of light emission. High magnetic fields provide another useful tool to infer the wave functions through magneto-tunneling [179] or luminescence spectroscopy [180].

For future applications, there has been also a lot of interest in quantum dots in the broad field of quantum information processing, with the use of QDs as single photon sources and biexcitonic states as sources of entagled photons [181]. Quantum dots in microcavities are also intensely investigated for realization of cavity quantum electrodynamics ideas and for studying light matter interaction in the strong coupling regime [182].

Finally, Ge/Si QDs have a type-II band alignment with holes localized in Ge and electrons constrained to be in the Si matrix. While the initial studies focused almost exclusively on type-I structures, type-II structures (other examples are GaSb/GaAs, InP/GaAs, ZnSe/ZnTe) have also attracted some attention, especially in the context of potential memory applications as well as for some fundamentally new physics.

VII. DEVICES, APPLICATIONS, AND NEW PHYSICS

The three-dimensional confinement of charge carriers in quantum dots and the consequent changes to the density of states have many favorable consequences for novel device applications and provide new opportunities for investigating light-matter interactions. In particular, self-assembled QDs offer a significant advantage over colloidal QDs because they can be rather easily integrated into typical semiconductor device structures. This allows the injection and extraction of charge carriers into the QDs with relative ease and also enables light to be efficiently coupled in or out of the QDs. Further, QDs offer higher material gain and radiative efficiency, improved temperature stability, and a better tolerance to defects. While the advantages of QDs for devices was predicted in the early 1980s [183,184], it has taken almost three decades of intensive research to achieve uniform, high-density, and defect-free QDs to realize many of the attractive features of QD devices.

There are two basic categories of devices based on

quantum dots. The first class uses the properties of large ensembles of QDs, mostly targeting applications in optoelectronics such as QD-based emitters and detectors: lasers, superluminescent diodes, optical amplifiers, and detectors. These include both devices based on band-to-band optical transitions, as well as intersubband transitions. More recent interest has been on another class of devices based on the properties of a single QD, especially the control of the emission of single photons from such devices, and also the possibility of triggered entangled-photon sources. These single-dot devices can enable applications in quantum information processing, cryptography, and possibly quantum computation. Another direction of research has been to study spin transport and relaxation within QDs, aimed at the development of spin-based electronics (spintronics), especially where a spin confined to a single QD can be used to define a quantum bit. In all these cases, device performance is critically linked to the size, shape, composition, doping level, uniformity, and density of the QDs, thus making the epitaxial growth process a key determinant for devices based on self-assembled QDs.

This section provides a brief overview of QD devices, with a specific focus on the materials and growth issues. A comprehensive review of the early work in QD devices is available in Ref. [5]. More recent reviews of the field are covered in books [9,12,13] and various topical review articles [18–23].

A. Quantum-Dot Lasers

Much of the initial work in QD devices was based on the promise of ultra-low threshold current density and temperature insensitivity of threshold current in QD lasers [183,184]. However, the early predictions assumed ideal, uniform QDs with d-function-like density of states, no surrounding semiconductor matrix, and one electron and hole state. In reality, self-assembled growth typically results in QDs with a spread in dot sizes and an associated wetting layer. In addition, the capping process needed to embed the QD in a higher bandgap semiconductor matrix leads to compositional grading at the interface, all of which result in inhomogeneous broadening. Control of the growth process is thus critical for QD-based laser structures. The first QD lasers were realized [185] only a decade after the initial prediction, although rapid progress thereafter soon resulted in lasers with record-low threshold current densities and temperature-stable operation. Much of the research in this field has been driven by the possibility of obtaining GaAs-based lasers operating at the $1.3-$ and $1.55-\mu$m telecommunications windows. In this wavelength region, the traditionally used InP-based quantum-well lasers have small band offsets and poor temperature sensitivity, and the lattice-matched InGaAsP and InGaAlAs material systems make the formation of Bragg mirrors for vertical cavity lasers difficult. Further InP substrates are more expensive, difficult to handle, and offer poorer heat sinking capability than GaAs substrates. For InGaAs/GaAs quantum wells to emit at 1.3 μm, a prohibitively high compressive strain limits pseudomorphic growth, and prevents their use in devices. However, for InAs QDs, island formation ensures structures of lower strain to form, and with the shift in energy due to quantum confinement, room-temperature operation in the near-infrared (IR) region is easily achieved. Further silicon is transparent in this wavelength region, thus making InAs QD devices interesting as sources for silicon-based integrated optics as well. In fact, the strain field around InAs QDs have been used as dislocation filters within buffer layers for the growth of GaAs on silicon [186]. To date, most monolithically grown III-V laser structures on silicon [186,187] and germanium [188] substrates are based on InAs QD active regions.

For low-threshold QD lasers, it is normally desirable to achieve lasing in the ground-state longest-wavelength optical transition. The optical gain depends on the density of QDs in the active region, and inversely on the spectral width of the optical transition. Thus, QD lasers require growth conditions that favor high areal density of uniform QDs. To provide adequate optical gain and enhance the confinement factor, most QD laser structures use multiple coupled layers of dots. Due to strain-driven self-alignment in the growth direction in multilayer QDs, dots in subsequent layers align to the larger dots in the underlying layers, as discussed earlier. Another important route for attaining high-density and long-wavelength luminescence for InAs QDs on GaAs substrates is the "dots-in-a-well" (DWELL) design [189–191]. (This is particularly important for QD-based photodetectors, discussed later.) In this method, the InAs QD is buried within a thin InGaAs quantum well (QW). The emission wavelength can be tuned by changing the composition and thickness of the QW while maintaining optimal growth conditions for the QDs, resulting in high uniform dot density and the best luminescent properties.

The state of the art in the performance of $1.2-$ to $1.3-\mu$m-emitting InAs QD lasers is exemplified by extreme low values of threshold current density of approximately 10 A cm^{-2} and internal losses of 0.25 cm^{-1} [192]. A summary of low threshold current density operation demonstrated in this wavelength range by various groups in shown in Figure 13. Devices optimized for high-power operation have shown 15.7 W CW power from a $200-\mu$m aperture [193]. A record-high operating temperature of 220 ^{o} for Fabry-Perot lasers and 150 ^{o}C for distributed feedback lasers has been demonstrated [194]. In these devices, a high density of dots (5.9×10^{10} cm^{-2}) coupled with a low full-width/half-maximum of the PL emission (24 meV at room temperature) was obtained by suppressing interdiffusion through optimization of the growth of the GaAs capping layer, thus enabling a very high modal gain to be obtained.

In an effort to push the emission of InGaAs QD lasers to longer wavelengths and reach the $1.55-\mu$m window,

various routes have been investigated, including the use of larger QD dimensions, changing the band discontinuity and strain by employing InGaAs confining layers, and growth on metamorphic buffer layers that reduce the strain in the QDs. The use of metamorphic buffer layers has been the most successful, with devices using InGaAs or GaAsSb layers, for example Ref. [195]. A detailed analysis of the various strain-engineering techniques for InAs QDs to achieve long-wavelength emission has been reported [196].

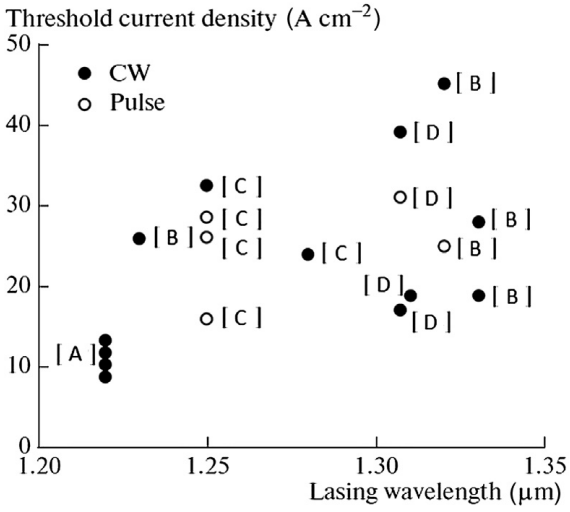

FIG. 13. Overview of state-of-the-art low-threshold current density operation of QD-based lasers based on GaAs substrates as a function of lasing wavelength, in continuous wave (CW, filled circles) or pulse (open circles) conditions. Data from research groups at Center for Research and Education in Optics and Lasers (CREOL), University of Central Florida (A); University of Texas-Austin (B); Center for High Technology Materials (CHTM), University of New Mexico (C); and University of Sheffield (D). Adapted from Zhukov et al. Ref. [22] and reproduced with permission.

Although most of the QD laser work has focused on near-IR devices based on InAs QDs on GaAs, there has also been a lot of effort on devices based on InAs or InGaAs QDs on InP substrates, where attaining 1.55-mm wavelength emission is easier (see Refs. [197,198] for reviews). For InP-based QD lasers, many initial results [199,200] were based on growth of InAs QDs on high-index InP planes such as (311)B, which offer a high density of nucleation points and allow for a high QD density. However, for device processing, (100)-oriented substrates are desirable, such as for ease of forming facets via cleaving. The growth of high-density, uniform InAs QDs on (100) InP has been more challenging, especially for MBE growth, with the self-assembled islands having a tendency for elongation along the [1-10] direction, leading to the formation of "quantum dashes." With optimized growth processes, high-performance results [201,202] have been demonstrated on (100) InP substrates as well. Growth on InP also allows extension of the emission wavelength toward the mid-IR region. By low-temperature growth of InAs QDs and a InGaAsP quaternary cap layer to minimize defect-related intermixing, laser emission at 1.95 mm has been shown [203]. Another approach to obtain emission around 2 μm has been the use of low-bandgap InAsSb QDs [204].

On the shorter wavelength side, there is extensive research on the use of InGaN QDs for lasers in the visible region. Although stimulated emission from GaN QDs was shown [205] in 1997, with improvements in the quality of nitride materials, especially due the availability of bulk GaN substrates with reduced defect density, electrically injected InGaN QD lasers in the green [206] and red [207] spectral region have been reported recently. This is an area where rapid developments would be expected in the near future. QD-based edge-emitting [132] and vertical cavity lasers [133] in the red region have also been reported from InP QDs embedded in an AlGaInP matrix.

B. Quantum-Dot-Based Superluminescent Diodes

Broadband light sources are useful for various applications, such as sources for wavelength division multiplexing, optical coherence tomography, fiber-optic sensors, and gyroscopes. The superluminescent diode (SLED) uses the internal amplification of spontaneous emission in a structure without optical feedback to prevent lasing and provides a convenient high brightness source with the broad optical spectrum of an LED. The few intrinsic drawbacks of QDs for diode lasers turn out to be actually advantageous for SLED operation [208,209]. In self-assembled QD systems, an unavoidable distribution in dot sizes leads to a dispersion in transition energies and hence an inhomogeneously broadened gain spectrum, which is useful for broadband sources. Furthermore, the limited density of states compared to QW devices arising from incomplete coverage of the surface, even at relatively high areal density, leads to a lower optical gain. This is a limitation for lasers, producing gain saturation and poor high-frequency response, but it is advantageous in delaying the onset of lasing in SLED devices. Similarly, simultaneous emission from both the excited state and ground state, although not desirable for a single mode laser, can be used to increase the emission bandwidth of a QD-based SLED.

The growth conditions during the deposition of the self-assembled QD layers can be adjusted to increase the distribution in dots sizes. For increasing the emission bandwidth even further, most designs use chirped multi-quantum-dot (CMQD) layers, with each layer of the QD stack having a slightly shifted center wavelength. This can be done by changing the dot composition, amount of material deposited to form the QD, or the material of the surrounding matrix [210,211]. Using these techniques, various groups have demonstrated GaAs- and InP-based QD SLEDs with > 100 nm bandwidth. With additional postgrowth thermal- or laser-based processing

to cause local intermixing of the QD layers, the emission bandwidth can be increased even further, with a record 360−nm-width emission being reported from InAs/InP CMQD structures [212].

C. Quantum-Dot Infrared Photodetectors

Another area where quantum dots have made a significant impact on device performance is in the detection of IR radiation, emerging as a competitive technology for imaging systems compared to existing quantum-well IR photodetectors (QWIPs) or detectors based on narrow-bandgap HgCdTe alloys (see reviews in Refs [23] and [213]). In QWIPs and quantum dot infrared photodetectors (QDIPs), infrared absorption occurs due to intersubband transitions from the ground state to various excited states in the QW or QD conduction band, respectively. Although QWIPs are well-established and large-area imaging systems are commercially available, their chief drawbacks are the inability to absorb normal incidence light (hence requiring special light coupling schemes, such as gratings or angled facets), a relatively high dark current, and operation limited to low temperatures [214–216]. The three-dimensional confinement of carriers within QDs provides an intrinsic solution to these issues. The selection rules for optical transitions in dots allow QDIPs to absorb normally incident radiation. Furthermore, the energy separations between levels within the dot are usually larger than the longitudinal optical (LO) phonon energy, reducing scattering and resulting in a longer carrier lifetime and consequently a significantly reduced dark current. The independence of the electronic distribution function on temperature in an ideal QD also means that QDIPs are better suited for operation at room temperature. Since the first demonstration [217] of a QDIP in 1998, there has been tremendous progress in device performance, driven largely by improvements in the growth of the QD layers and new device design concepts. QDIPs have demonstrated room temperature operation in the midwave ($3-5\,\mu$m), longwave ($8-12\,\mu$m), and very longwave (VLWIR, $>14\,\mu$m) IR regions [218] [219], and to 150 K in the far IR and terahertz (THz) regions [220]. The DWELL design (see Ref. [221] for a review), in which the IR absorption transitions from the QD ground state to states in the QW can be selectively used, has proven to be extremely beneficial for QDIPs. For a fixed QD ground state, the QW composition and thickness can be varied in order to precisely tailor the peak wavelength. This also permits controlled multiwavelength operation by selecting different transitions by changing the detector bias voltage. The pioneering development of a three-color DWELL detector by Krishna et al. [221] is shown in Figure 14. Other QDIP designs to improve performance include the use of superlattices [222] and resonant tunneling structures [223].

The parameters for the growth of the self-assembled QD stacks and DWELL structures are critical in determining the device performance. There are various choices for QD material system, dot size and doping density, continuous or pulsed growth mode, capping layer material, etc.; tradeoffs often need to be made to optimize overall performance [23]. For example, InAs QDs offer better carrier confinement, but the stronger potential well impedes carrier extraction. Using InGaAs QDs, as favored for VLWIR devices, allows easier carrier extraction, at the cost of higher dark currents due to the poorer confinement. Large-sized QDs having a smaller energy level separation between the subbands are favored for devices in the far IR and THz regions, but the QD density is usually reduced for large-sized dots. Smaller QDs provide a higher dot density, which improves absorption. Similarly, the choice of doping within the QDs presents another area of compromise. Adequate carriers are needed to achieve efficient absorption, but high doping levels or unintentional doping of the wetting layer during QD growth contribute to increased dark current. In the case of DWELL structures, the optimal growth temperatures for the InGaAs QW and the InAs QD are similar, unlike for InAs QDs capped with GaAs. However, the InGaAs QW increases the overall compressive strain, thus limiting the maximum number of stacks that can be grown before the formation of defects degrades material quality. Thus, optimizing the various growth parameters, usually via systematic AFM and PL investigations, to obtain the QDs with excellent optical quality and the appropriate size and density for the desired operational wavelength(s) is vital.

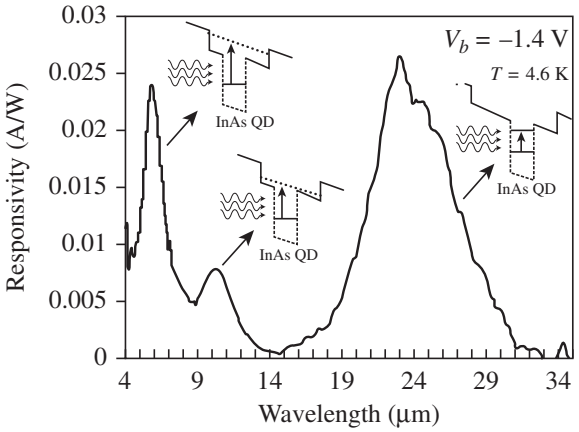

FIG. 14. Three-color photoresponse from a 10-layer $InAs/In_{0.15}Ga_{0.85}As$ DWELL type QDIP detector. The arrows point to the schematic of the electronic transitions that give rise to the respective peaks. The mid-IR peak at around $5\,\mu$m arises from a transition from a state in the QD to a quasi-bound state close to the top of the QW, whereas the peak at $10\,\mu$m is a transition from a bound state in the dot to a bound state in the QW. The far IR peak around $25\,\mu$m is from transitions between two states in the QD. From Krishna et al. [221] ©IOP Publishing 2005. Reproduced with permission.

Over the years, developments in QDIPs have shown lower dark current and hence higher operating temperature than in QWIPs, resulting in background limited perfor- mance at higher temperatures. Large QDIP focal plane arrays [224] operating in the range of thermoelectric coolers and four-color operation [225] have been demonstrated.

Detectors based on intersubband transitions in III-nitride QDs are an area of recent interest (see Ref. [226] for a review) because the large conduction-band offset (1.8 eV for GaN/AlN QDs) results in the intersubband transitions lying in the near-IR region covering the $1.3-1.6\,\mu$m wavelength optical communication windows. The larger band gaps also reduce carrier leakage, improving high-temperature operation. QDIPs based on plasma-MBE grown GaN/AlN QDs stacks have demonstrated room-temperature detection at $1.4-\mu$m wavelength [227]. Furthermore, the large energy of the LO phonon (92 meV) in GaN allows devices to be designed in the $5-10$ THz band, inaccessible to InAs-based QDs due to phonon absorption. However, control of polarization-induced internal electric fields in the III-nitrides still presents a major challenge to extending the intersubband devices to longer wavelengths.

D. Quantum-Dot-Based Memory Devices

There have been many experiments to show that single charges can be electrically [228,229] or optically [230,231] injected into QDs. Furthermore, the effects of a QD layer on the transport properties of a 2D electron gas in a modulation-doped field-effect transistor (MODFET) geometry have also been studied [228,232]. Based on these, a nonvolatile protoype memory "QD-Flash" combining charge storage with a MODFET to access the information has been developed [233]. Preliminary results are encouraging, with more than 1-s storage times measured at room temperature for InAs-based QDs and more than 10-year storage times predicted using novel material combinations such as GaSb/AlAs QDs [234]. Although proof-of-principle QD memory devices have been demonstrated at low temperatures (85 K for InAs/GaAs QDs, 220 K for $InAs/Al_{0.9}Ga_{0.1}As$ QDs) [233], a lot of improvement in storage lifetime and read/write/erase times is still needed for commercial viability. The strong optical sensitivity of these structures also allows for the development of QD phototransistors with single-photon counting capabilities [235].

E. Quantum-Dot-Based Spin Devices

The strong 3D confinement in quantum dots also results in spin states that are, at least theoretically, expected to be more robust against decoherence compared to bulk materials [11,236,237]. This makes self-assembled QDs potential candidates for various spintronic applications and also for use in quantum information processing, where a spin confined to the QD can serve as a quantum bit. The main challenges in realizing spin-based applications using QDs are in the injection of polarized spins, a spin reservoir such as a ferromagnetic material, storage of the spin in the QD, and appropriate techniques to manipulate and read out the spin orientation.

F. Single Quantum-Dot Devices

To study and use the "artificial atom"-like properties of quantum dots, measurements are mostly required to be made on a single isolated QD rather than a dense ensemble of them. Single QDs have also been used to generate polarization-entangled photon pairs, study the coupling between a single QD and a photonic cavity, and manipulate single-electron spins in QDs [11,12,238]. Much of this has been possible due to the prevalence of and improvements in nanofabrication techniques, allowing ultra-small cavities with high-quality factors to be coupled to QDs. In many cases, the QDs are formed by a combination of self-assembled growth along with top-down lithographic techniques, which offer control of the spatial location of the dot as well.

Typically, self-assembled QD ensembles have an areal density of a few 10^9-10^{10} cm^{-2}, and a large density has been desired for most optoelectronic applications. However, for studying single QDs, the easiest route has been to control the self-assembly process to achieve a low surface density, typically $< 10^8$ cm^{-2}, so that the dots are far enough apart that they can be individually optically addressed [239]. Most groups attempt to stop the QD material deposition just after the onset of the 2D-3D growth transition and control deposition parameters such as growth rate, temperature, and growth interrupts to control the dot density.

Since the first report of single-photon emission from a single QD, single-photon sources have been developed in various QD systems, ranging from the ultraviolet to the near IR. The comprehensive volume by Michler et al. [12] details the progress that has been made in addressing critical issues such as coherent state preparation, obtaining polarization control and high repetition rates, and designing cavity structures for low electrical pump currents and enhanced photon collection efficiency. However, commercial application of single QD devices still requires many challenges to be overcome, primarily increasing operation temperatures at least to levels that can be easily obtained via thermoelectric cooling.

VIII. SUMMARY AND OUTLOOK

What was initially an annoyance associated with a growth instability in strained epitaxy has matured into one of the most exciting and intensively studied areas in semi- conductor crystal growthself-assembled quantum

dots. With painstaking experimental work supported by theoretical and computational modeling, the strain-mediated self- assembly and the Stranski-Krastanov transition have been documented with unprece- dented atomic-scale detail for a variety of conditions and material systems. In this review, we have attempted to give an overview of the growth processes, as well as the fundamental correlations between structure and functionality, which are key to the use of these QDs in various technologically relevant applications. We have briefiy shown how the basic knowledge gained from understanding the self-assembly process coupled with innovations in characterization has led to more ambitious ideas of 2D and 3D ordering of QDs, and to the improvement in uniformity in size and density of quantum dots. We have highlighted a range of devices where the use of QDs can provide improved per- formance and functionality. For lasers, although QDs are intrinsically superior than the currently used quantum- well devices, it is difficult to achieve the necessary gain at reduced pump levels when sample inhomogeneities are taken into account. Hence, advances in growth control to reduce the inhomogeneous broadening are still needed before QD-based devices find widespread use. Most of what has been covered relates to the use of ensembles of QDs. The laboratory-level demonstrations of utilizing spin or charge degrees of freedom, single photon emission, etc. in single quantum dots clearly show the rich physics that can be exploited for new devices. Single QD devices are unlikely to be achieved using self-assembly alone. However, the nanoscale fabrication technology and templating schemes available today, coupled with the current understanding and control over materials growth, makes rapid progress in this area seem inevitable. From the view of the crystal grower, the combination of self-assembly, vertical stacking, pattern-controlled positioning of islands, and wide choice of semiconductor materials provides a unique toolbox for the synthesis of fully controlled three-dimensional nanostructures.

[1] Goldstein L, Glas F, Marzin JY, Charasse MN, Le Roux G. Appl Phys Lett 1985;47:1099. http://dx.doi.org/10.1063/1.96342.

[2] Eaglesham DJ, Cerullo M. Phys Rev Lett 1990;64:1943. http://dx.doi.org/10.1103/PhysRevLett.64.1943.

[3] Guha S, Madhukar A, Rajkumar KC. Appl Phys Lett 1990;57:2110. http://dx.doi.org/10.1063/1.103914.

[4] Mo Y-W, Savage DE, Swartzentruber BS, Lagally MG. Phys Rev Lett 1990;65:1020. http://dx.doi.org/10.1103/PhysRevLett.65.1020.

[5] Bimberg D, Grundmann M, Ledentsov NN. Quantum dot heterostructures. Wiley; 1999. ISBN: 978-0-471-97388-1.

[6] Grundmann M, editor. Nano-optoelectronics, concepts, physics and devices. Springer; 2002. ISBN: 3540433945.

[7] Joyce BA, Kelires PC, Naumovets AG, Vvedensky DD, editors. Quantum dots: fundamentals, applications, and frontiers. Dordrecht: Springer; 2005. ISBN 978-1-4020-3313-1.

[8] Schmidt OG, editor. Lateral alignment of epitaxial quantum dots, Springer series on nanoscience and technology. Springer; 2007. ISBN: 978-3-540-46935-3.

[9] Henini M, editor. Handbook of self assembled semiconductor nanostructures for novel devices in photonics and electronics. Elsevier; 2011. ISBN: 0080560474.

[10] Jacak L, Hawrylak P, Wojs A. Quantum dots. Springer; 1998. ISBN: 3540636536.

[11] Gywat O, Krenner HJ, Berezovsky J. Spins in optically active quantum dots: concepts and methods. Wiley; 2009. ISBN: 3527408061.

[12] Michler P. Single semiconductor quantum dots. Springer; 2009. ISBN 978-3-540-87445-4.

[13] Wang ZM. Quantum dot devices. Springer; 2012. ISBN 978-1-4614-3569-3.

[14] Sugawara M, editor. Self-assembled InGaAs/GaAs quantum dots. Willardson RK, Weber ER, editors. Semiconductors and semimetals, vol. 60. Elsevier; 1999. ISBN: 0-12-752169-0.

[15] Biehl M, Much F, Vey C. "Off-lattice Kinetic Monte Carlo Simulations of Strained Heteroepitaxial Growth", Chapter 4. In: Voigt A, editor. Multiscale modeling in epitaxial growth. Birkhäuser Basel; 2005. ISBN: 978-3-7643-7208-8.

[16] Stangl J, Holy V, Bauer G. Rev Mod Phys 2004;76:725. http://dx.doi.org/10.1103/RevModPhys.76.725.

[17] Seifert W, Carlsson N, Miller M, Pistol M-E, Samuelson L, Wallenberg LR. Prog Cryst Growth Charact Mater 1996;33:423. http://dx.doi.org/10.1016/S0960-8974(96)00090-3.

[18] Yoffe AD. Adv Phys 2001;50(1). http://dx.doi.org/10.1080/00018730010006608.

[19] Skolnick MS, Mowbray DJ. Ann Rev Mater Res 2004;34:181. http://dx.doi.org/10.1146/annurev.matsci.34.082103.133534.

[20] Bhattacharya P, Ghosh S, Stiff-Roberts AD. Ann Rev Mater Res 2004;34:1. http://dx.doi.org/10.1146/annurev.matsci.34.040203.111535.

[21] Petroff PM. Adv Mater 2011;23:2372. http://dx.doi.org/10.1002/adma.201100275.

[22] Zhukov AE, Maksimov MV, Kovsh AR. Semiconductors 2012;46:1225. http://dx.doi.org/10.1134/S1063782612100223.

[23] Barve AV, Krishna S. Quantum dot infrared photodetectors. In: Gunapala SD, Rhiger DR, Jagadish C, editors. Semiconductors and semimetals, vol. 84. San Diego: Academic Press; 2011. p. 153. ISBN: 978-0-12-381337-4.

[24] Chow WW, Jahnke F. Prog Quantum Electron 2013;37:109. http://dx.doi.org/10.1016/j.pquantelec.2013.04.001.

[25] Aqua J-N, Berbezier I, Favre L, Frisch T, Ronda A. Phys Rep 2013;522:59. http://dx.doi.org/10.1016/j.physrep.2012.09.006.

[26] Joyce BA, Vvedensky DD. Mater Sci Eng 2004;46:127. http://dx.doi.org/10.1016/j.mser.2004.10.001.

[27] Placidi E, Arciprete F, Fanfoni M, Patella F, Orsini E, Balzarotti A. J Phys Condens Matter 2007;19: 225006. http://dx.doi.org/10.1088/0953-8984/19/22/225006.

[28] Leonard D, Pond K, Petroff PM. Phys Rev B 1994;50:11687. http://dx.doi.org/10.1103/PhysRevB.50.11687.

[29] Penev E, Stojković S, Kratzer P, Scheffler M. Phys Rev B 2004;69:115335. http://dx.doi.org/10.1103/PhysRevB.69.115335.

[30] Shen X-Q, Kishimoto D, Nishinaga T. Jpn J Appl Phys 1994;33:11. http://dx.doi.org/10.1143/JJAP.33.11.

[31] Frank FC, Van der Merwe JH. Proc R Soc Lond A Math Phys Sci 1949;198:205.

[32] Volmer M, Weber A. Z Phys Chem (Munich) 1926;119:277.

[33] Stranski IN, Krastanov L. Sitzungsber Akad Wiss Wien, Math-Naturwiss Kl Abt 2B 1938;146:797.

[34] Venables JA. Introduction to surface and thin film phenomena. Cambridge University Press; 2000. ISBN: 0521785006.

[35] Kolasinski KW. Surface science, foundations of catalysis and nanoscience. 3rd ed. Wiley; 2012. http://dx.doi.org/10.1002/9781119941798.ch1.

[36] Matthews JW, Blakeslee AE. J Cryst Growth 1974;27:118. http://dx.doi.org/10.1016/S0022-0248(74)80055-2.

[37] Kubin LP. "Dislocations and stress relaxation in heteroepitaxial films". In: Hanbücken M, Deville J- P, editors. Stress and strain in epitaxy. Elsevier; 2001. ISBN: 978-0-444-50865-2.

[38] Pimpinelli A, Villain J. Physics of crystal growth. Cambridge; 1998. ISBN: 0521551986.

[39] Krug J, Michely T. Islands, mounds, and atoms: patterns and processes in crystal growth far from equilibrium. Springer; 2004. ISBN: 3540407286.

[40] Srolovitz DJ. Acta Metall 1989;37:621. http://dx.doi.org/10.1016/0001-6160(89)90246-0.

[41] Johansson J, Seifert W. J Cryst Growth 2002;234:132. http://dx.doi.org/10.1016/S0022-0248(01) 01674-8.

[42] Snyder CW, Mansfield JF, Orr BG. Phys Rev B 1992;46:9551. http://dx.doi.org/10.1103/PhysRevB.46.9551.

[43] Heyn Ch. Phys Rev B 2001;64:165306. http://dx.doi.org/10.1103/PhysRevB.64.165306.

[44] Heitz R, Ramachandran TR, Kalburge A, Xie Q, Mukhametzhanov I, Chen P, et al. Phys Rev Lett 1997;78:4071. http://dx.doi.org/10.1103/PhysRevLett.78.4071.

[45] Cullis AG, Norris DJ, Walther T, Migliorato MA, Hopkinson M. Phys Rev B 2002;66(081305(R)). http://dx.doi.org/10.1103/PhysRevB.66.081305.

[46] Shchukin VA, Ledentsov NN, Kopev PS, Bimberg D. Phys Rev Lett 1995;75:2968. http://dx.doi.org/10.1103/PhysRevLett.75.2968.

[47] Daruka I, Barabaśi A-L. Phys Rev Lett 1997;79:3708. http://dx.doi.org/10.1103/PhysRevLett.79.3708.

[48] Petroff PM, DenBaars SP. Superlattices Microstruct 1994;15(15). http://dx.doi.org/10.1006/spmi.1994.1004.

[49] Müller-Kirsch L, Heitz R, Pohl UW, Bimberg D, Haüsler I, Kirmse H, et al. Appl Phys Lett 2001;79:1027. http://dx.doi.org/10.1063/1.1394715.

[50] Bansal B, Gokhale MR, Bhattacharya A, Arora BM. J Appl Phys 2007;101:094303. http://dx.doi.org/10.1063/1.2710292.

[51] Priester C, Lannoo M. Phys Rev Lett 1995;75:93. http://dx.doi.org/10.1103/PhysRevLett.75.93.

[52] Liu F, Li AH, Lagally MG. Phys Rev Lett 2001;87:126103. http://dx.doi.org/10.1103/PhysRevLett.87.126103.

[53] Politi P, Grenet G, Marty A, Ponchet A, Villain J. Phys Rep 2000;324:271. http://dx.doi.org/10.1016/S0370-1573(99)00046-0.

[54] Daruka I, Tersoff J, Barabasi A-L. Phys Rev Lett 1997;82:2753. http://dx.doi.org/10.1103/PhysRevLett.82.2753.

[55] Jesson DE, Chen G, Chen KM, Pennycook SJ. Phys Rev Lett 1998;80:5156. http://dx.doi.org/10.1103/PhysRevLett.80.5156.

[56] Wang LG, Kratzer P, Schef?er M, Moll N. Phys Rev Lett 1999;82:4042. http://dx.doi.org/10.1103/PhysRevLett.82.4042.

[57] Henini M. Dilute nitride semiconductors. Elsevier; 2005. ISBN: 978-0-08-044502-1.

[58] Hull R, Bean JC, editors. Germanium silicon: physics and materials. Semiconductors and semimetals, vol. 56. Academic Press; 1998. ISBN-10: 012752164X.

[59] Shchukin VA, Ledentsov NN, Bimberg D. Epitaxy of nanostructures. Berlin: Springer; 2004. ISBN: 9783540678175.

[60] Bansal B, Gokhale MR, Bhattacharya A, Arora BM. Appl Phys Lett 2005;87:203104. http://dx.doi.org/10.1063/1.212848.

[61] DobbsHT, Vvedensky DD, Zangwill A, Johansson J, Carlsson N, SeifertW. Phys Rev Lett 1997;79:897. http://dx.doi.org/10.1103/PhysRevLett.79.897.

[62] Christiansen SH, Schmidbauer M, Wawra H, Schneider R, Neumann W, Strunk HP. Energetics and Kinetics of Self-Organized Structure Formation in Solution Growth – the SiGe/Si System. In: Schmidt OG, editor. Lateral alignment of epitaxial quantum dots. Springer; 2007. ISBN: 978-3-540- 46935-3.

[63] Venables JA, Spiller GDT, Hanbucken M. Rep Prog Phys 1984;47:399. http://dx.doi.org/10.1088/0034-4885/47/4/002.

[64] Krzyzewski TJ, Joyce PB, Bell GR, Jones TS. Phys Rev B 2002;66(201302(R)). http://dx.doi.org/10.1103/PhysRevB.66.201302.

[65] Dubrovskii VG, Cirlin GE, Musikhin YuG, Samsonenko YuB, Tonkikh AA, Polyakov NK, et al. J Cryst Growth 2004;267:47. http://dx.doi.org/10.1016/j.jcrysgro.2004.03.055.

[66] Barabasi A-L, Stanley HE. Fractal concepts in surface growth. Cambridge; 1995. ISBN: 9780521483186.

[67] Joyce BA, Vvedensky DD. Mater Sci Eng Rep 2004;46:127. http://dx.doi.org/10.1016/j.mser.2004.10.001.

[68] Amar JG, Family F. Phys Rev Lett 1995;74:2066. http://dx.doi.org/10.1103/PhysRevLett.74.2066.

[69] Bartelt MC, Tringides MC, Evans JW. Phys Rev B 1993;47:13891. http://dx.doi.org/10.1103/PhysRevB.47.13891.

[70] Zinke-Allmang M. Thin Solid Films 1999;346:1. http://dx.doi.org/10.1016/S0040-6090(98)01479-5.

[71] Bressler-Hill V, Varma S, Lorke A, Nosho BZ, Petroff PM, Weinberg WH. Phys Rev Lett 1995; 74:3209.

http://dx.doi.org/10.1103/PhysRevLett.74.3209.
[72] Ebiko Y, Muto S, Suzuki D, Itoh S, Shiramine K, Haga T, et al. Phys Rev Lett 1998;80:2650. http://dx.doi.org/10.1103/PhysRevLett.80.2650.
[73] Cao YG, Xie MH, Liu Y, Xu SH, Ng YF, Wu HS, et al. Phys Rev B 2003;68:161304. http://dx.doi.org/10.1103/PhysRevB.68.161304.
[74] Miyamoto S, Moutanabbir O, Haller EE, Itoh KM. Phys Rev B 2009;79:165415. http://dx.doi.org/10.1103/PhysRevB.79.1615415.
[75] Pimpinelli A, Einstein TL. Phys Rev Lett 2007;99:226102. http://dx.doi.org/10.1103/PhysRevLett.99.226102.
[76] Xie Q, Madhukar A, Chen P, Kobayashi NP. Phys Rev Lett 1995;75:2542. http://dx.doi.org/10.1103/PhysRevLett.75.2542.
[77] Tersoff J, Teichert C, Lagally TG. Phys Rev Lett 1996;76:1675. http://dx.doi.org/10.1103/PhysRevLett.76.1675.
[78] Kamath K, Chervela N, Linder KK, Sosnowski T, Jiang H-T, Norris T, et al. Appl Phys Lett 1997;71: 927. http://dx.doi.org/10.1063/1.119691.
[79] Wasilewski ZR, Fafard S, McCaffrey JP. J Cryst Growth 1999;201:1131. http://dx.doi.org/10.1016/S0022-0248(98)01539-5.
[80] Fafard S, Wasilewski ZR, Allen CNi, Picard D, Spanner M, McCaffrey JP, et al. Phys Rev B 1999;59: 15368. http://dx.doi.org/10.1103/PhysRevB.59.15368.
[81] Steimetz E, Wehnert T, Kirmse H, Poser F, Zettler J-T, Neumann W, et al. J Cryst Growth 2000;221:592. http://dx.doi.org/10.1016/S0022-0248(00)00784-3.
[82] Hospodková A, Vyskočil J, PangraćJ, Oswald J,Hulicius E, Kuldová K. Surf Sci 2010;604:318. http://dx.doi.org/10.1016/j.susc.2009.11.023.
[83] González JC, Magalhães-Paniago R, Rodrigues WN, Malachias A, Moreira MVB, de Oliveira AG, et al. Appl Phys Lett 2001;78:1056. http://dx.doi.org/10.1063/1.1347024.
[84] Yang B. J Appl Phys 2002;92:3704. http://dx.doi.org/10.1063/1.1506386.
[85] Yang B, Tewary VK. Phys Rev B 2003;68:035301. http://dx.doi.org/10.1103/PhysRevB.68.035301.
[86] Leon R, Senden TJ, Kim Y, Jagadish C, Clark A. Phys Rev Lett 1997;78:4942. http://dx.doi.org/10.1103/PhysRevLett.78.4942.
[87] Brunner K, Zhu J, Miesner C, Abstreiter G, Kienzle O, Ernst F. Phys E 2000;7:881. http://dx.doi.org/10.1016/S1386-9477(00)00081-3.
[88] Poser F, Bhattacharya A, Weeke S, Richter W. J Cryst Growth 2003;248:317. http://dx.doi.org/10.1016/S0022-0248(02)01886-9.
[89] Luedtke WD, Landman U. Phys Rev B 1991;44:5970. http://dx.doi.org/10.1103/PhysRevB.44.5970.
[90] Chkoda L, Schneider M, Shklover V, Kilian L, Sokolowski M, Heske C, et al. Chem Phys Lett 2003; 371:548. http://dx.doi.org/10.1016/S0009-2614(03)00297-5.
[91] Koch R. J Phys Condens Matter 1994;6:9519. http://dx.doi.org/10.1088/0953-8984/6/45/005.
[92] Brunner Karl. Rep Prog Phys 2002;65:27. http://dx.doi.org/10.1088/0034-4885/65/1/202.
[93] Aqua J-N, Berbezier I, Favre L, Frisch T, Ronda A. Phys Rep 2013;522:59. http://dx.doi.org/10.1016/j.physrep.2012.09.006.
[94] Berbezier I, Ronda A. Surf Sci Rep 2009;64:47. http://dx.doi.org/10.1016/j.surfrep.2008.09.003.
[95] Bean JC, Feldman LC, Fiory AT, Nakahara S, Robinson IK. J Vac Sci Technol 1984;A2:436. http://dx.doi.org/10.1116/1.572361.
[96] Takagahara T. Phys Rev B 1992;46:15578. http://dx.doi.org/10.1103/PhysRevB.46.15578.
[97] Medeiros-Ribeiro G, Bratkovski AM, Kamins TI, Ohlberg DAA, Williams RS. Science 1998;279:353. http://dx.doi.org/10.1126/science.279.5349.353.
[98] Ross FM, Tromp RM, Reuter MC. Science 1996;271:933. http://dx.doi.org/10.1126/science.286.5446.1931.
[99] Daruka I, Tersoff J, Barabasi AL. Phys Rev Lett 1997;83:2753. http://dx.doi.org/10.1103/PhysRevLett.83.2753.
[100] Rastelli A, Stoffel M, Tersoff J, Kar GS, Schmidt OG. Phys Rev Lett 2005;95:026103. http://dx.doi.org/10.1103/PhysRevLett.95.026103.
[101] Ross FM, Tersoff J, Tromp RM. Phys Rev Lett 1998;80:984. http://dx.doi.org/10.1103/PhysRevLett.80.984.
[102] Rastelli A, Kummer M, Von Känel H. Phys Rev Lett 2001;87(25):256101. http://dx.doi.org/10.1103/PhysRevLett.87.256101.
[103] Lan H, Ding Y. Nano Today 2012;7(2):94. http://dx.doi.org/10.1016/j.nantod.2012.02.006.
[104] Lorke A, Garcia JM, Blossey R, Luyken RJ, Petroff PM. Self-Organized InGaAs Quantum Rings – Fabrication and Spectroscopy. In: Kramer B, editor. Advances in solid state physics, vol. 43. Springer; 2003. p. 125. ISBN 978-3-540-40150-6.
[105] Heyn C, Stemmann A, Hansen W. Self-Assembly of Quantum Dots and Rings on Semiconductor Surfaces. In: Heitmann D, editor. Quantum materials. Springer; 2010. p. 1. ISBN: 9783642105524.
[106] Chichibu S, Azuhata T, Sota T, Nakamura S. Appl Phys Lett 1996;69:4188. http://dx.doi.org/10.1063/1.116981.
[107] Narukawa Y, Kawakami Y, Funato M, Fujita S, Fujita S, Nakamura S. Appl Phys Lett 1997;70:981. http://dx.doi.org/10.1063/1.118455.
[108] Graham DM, Soltani-Vala A, Dawson P, Godfrey MJ, Smeeton TM, Barnard JS, et al. J Appl Phys 2005;97:103508. http://dx.doi.org/10.1063/1.1897070.
[109] De S, Das DK, Layek A, Raja A, Singh MK, Bhattacharya A, et al. Appl Phys Lett 2011;99:251911. http://dx.doi.org/10.1063/1.3671092.
[110] Tanaka S, Iwai S, Aoyagi Y. Appl Phys Lett 1996;69:4096. http://dx.doi.org/10.1063/1.117830.
[111] Daudin B, Widmann F, Feuillet G, Samson Y, Arlery M, Rouvie re JL. Phys Rev B 1997;56:7069. http://dx.doi.org/10.1103/PhysRevB.56.7069.
[112] Miyamura M, Tachibana K, Arakawa Y. Appl Phys Lett 2002;80:3937. http://dx.doi.org/10.1063/1.1482416.
[113] Paskova T. Phys Stat Solidi B 2008;245(6):1011. http://dx.doi.org/10.1002/pssb.200743274.
[114] Marquardt O, Hickel T, Neugebauer J. J Appl Phys 2009;106:083707. http://dx.doi.org/10.1063/1.3246864.
[115] Founta S, Rol F, Bellet-Amalric E, Bleuse J, Daudin B, Gayral B, et al. Appl Phys Lett 2005;86: 171901. http://dx.doi.org/10.1063/1.1905807.
[116] Schulz S, Berube A, OReilly EP. Phys Rev B 2009;79(081401(R)). http://dx.doi.org/10.1103/PhysRevB.79.081401.

[117] Dimitrakopulos GP, Kalesaki E, Kioseoglou J, Kehagias Th, Lotsari A, Lahourcade L, et al. J Appl Phys 2010;108:104304. http://dx.doi.org/10.1063/1.3506686.

[118] Das A, Dimitrakopulos GP, Kotsar Y, Lotsari A, Kehagias Th, Komninou Ph, et al. Appl Phys Lett 2011;98:201911. http://dx.doi.org/10.1063/1.3588335.

[119] Daudin B, Adelmann C, Gogneau N, Sarigiannidou E, Monroy E, Fossard F, et al. Physica E Low Dimens Syst Nanostruct 2004;21(24):540. http://dx.doi.org/10.1016/j.physe.2003.11.075.

[120] Rouviere J-L, Bougerol C, Amstatt B, Bellet-Almaric E, Daudin B. Appl Phys Lett 2008;92:201904. http://dx.doi.org/10.1063/1.2917449.

[121] Coraux J, Amstatt B, Budagoski JA, Bellet-Amalric E, Rouviér J-L, Favre-Nicoli V, et al. Phys Rev B 2006;74:195302. http://dx.doi.org/10.1103/PhysRevB.74.195302.

[122] Klude M, Passow T, Kro ger R, Hommel D. Electron Lett 2001;37:1119. http://dx.doi.org/10.1049/el:20010764.

[123] Xin SH, Wang PD, Yin A, Kim C, Dobrowolska M, Merz JL, et al. Appl Phys Lett 1996;69:3884. http://dx.doi.org/10.1063/1.117558.

[124] Tinjod F, Gilles B, Moehl S, Kheng K,Mariette H. Appl Phys Lett 2003;82:4340. http://dx.doi.org/10.1063/1.1583141.

[125] Pohl UW, Engelhardt R, Tu rck V, Bimberg D. J Cryst Growth 1998;195:569. http://dx.doi.org/10.1016/S0022-0248(98)00709-X.

[126] Mackowski S. Thin Solid Films 2002;412:96. http://dx.doi.org/10.1016/S0040-6090(02)00319-X.

[127] Kratzert PR, Puls J, Rabe M, Henneberger F. Appl Phys Lett 2001;79:2814. http://dx.doi.org/10.1063/1.1413735.

[128] Titova LV, Furdyna JK, Dobrowolska M, Lee S, Topuria T, Moeck P, et al. Appl Phys Lett 2002; 80:1237. http://dx.doi.org/10.1063/1.1450254.

[129] Lee S, Daruka I, Kim CS, Barabasi AL, Merz JL, Furdyna JK. Phys Rev Lett 1998;81:3479. http://dx.doi.org/10.1103/PhysRevLett.81.3479.

[130] Seifert W, Carlsson N, Miller M, Pistol M-E, Samuelson L, Wallenberg L. Prog Cryst Growth Charact Mater 1996;33:423. http://dx.doi.org/10.1049/el:20010764.

[131] Persson J, Holm M, Pryor C, Hessman D, Seifert W, Samuelson L, et al. Phys Rev B 2003; 67(3):035320. http://dx.doi.org/10.1103/PhysRevB.67.035320.

[132] Schulz W-M, Eichfelder M, Robach R, Jetter M, Michler P. J Cryst Growth 2011;315:123. http://dx.doi.org/10.1016/j.jcrysgro.2010.07.018.

[133] Schwarzback T, Bek R, Hargart F, Kessler CA, Kahle H, Koroknay E, et al. Appl Phys Lett 2013;102: 092101. http://dx.doi.org/10.1063/1.4793299.

[134] Lee JW, Schremer AT, Fekete D, Shealy JR, Ballantyne JM. J Electron Mater 1997;26:1199. http://dx.doi.org/10.1007/s11664-997-0020-0.

[135] Porsche J, Scholz F. J Cryst Growth 2000;221:571. http://dx.doi.org/10.1016/S0022-0248(00)00780-6.

[136] Datta S, Bhattacharya A, Gokhale MR, Pai SP, John J, Arora BM. J Cryst Growth 2002;241:115. http://dx.doi.org/10.1016/S0022-0248(02)01207-1.

[137] Pietsch U, Holy V, Baumbach T. In: High-resolution X-ray scattering: from thin films to lateral nanostructures. Tracts in modern physics. 2nd ed, vol. 149. Springer; 2004 [chapter 14]. ISBN 978-0-387-40092-1.

[138] Eisele H, Flebbe O, Kalka T, Preinesberger C, Heinrichsdorff F, Krost A, et al. Appl Phys Lett 1999;75:106. http://dx.doi.org/10.1063/1.124290.

[139] Liu N, Tersoff J, Baklenov O, Holmes Jr AL, Shih CK. Phys Rev Lett 2000;84:334. http://dx.doi.org/10.1103/PhysRevLett.84.334.

[140] Bruls DM, Koenraad PM, Salemink HWM, Wolter JH, Hopkinson M, Skolnick MS. Appl Phys Lett 2003;82:3758. http://dx.doi.org/10.1063/1.1578709.

[141] Rosenauer A, Fischer U, Gerthsen D, Förster A. Appl Phys Lett 1997;71:3868. http://dx.doi.org/10.1063/1.120528.

[142] Kret S, Benabbas T, Delamarre C, Androussi Y, Doubon A, Laval JY, et al. J Appl Phys 1999;86:1988. http://dx.doi.org/10.1063/1.370998.

[143] Rosenauer A, Gerthsen D. Ultramicroscopy 1999;76:49. http://dx.doi.org/10.1016/S0304-3991(98)00067-9.

[144] Miller PD, Liu C-M, Henstrom WL, Gibson JM, Huang Y, Zhang P, et al. Appl Phys Lett 1999;75:46. http://dx.doi.org/10.1063/1.124272.

[145] Henstrom WL, Liu C-P, Gibson JM, Kamins TI,Williams RS. Appl Phys Lett 2000;77:1623. http://dx. doi.org/10.1063/1.1309027.

[146] Kisielowski C, Schwander P, Bauman FH, Seibt M, Kim Y, Ourmazd A. Ultramicroscopy 1995; 58:131. http://dx.doi.org/10.1016/0304-3991(94)00202-X.

[147] Schmidbauer M, Hanke M, Ko hler R. Cryst Res Technol 2002;36:1. http://dx.doi.org/10.1002/1521-4079(200202)37:1¡3::AID-CRAT3¿3.0.CO;2-9.

[148] Headrick RL, Baribeau J-M. Phys Rev B 1993;48:9174. http://dx.doi.org/10.1103/PhysRevB.48.917.

[149] Kondrashkina EA, Stepanov SA, Opitz R, Schmidbauer M, Ko hler R, Hey R, et al. Phys Rev B 1997; 56:10469. http://dx.doi.org/10.1103/PhysRevB.56.10469.

[150] Hesse A, Stangl J, Holy V, Roch T, Bauer G, Schmidt OG, et al. Phys Rev B 2002;66:085321. http://dx.doi.org/10.1103/PhysRevB.66.085321.

[151] Kegel I, Metzger TH, Lorke A, Peisl J, Stangl J, Bauer G, et al. Phys Rev Lett 2000;85:1694. http://dx.doi.org/10.1103/PhysRevLett.85.1694.

[152] Kegel I, Metzger TH, Lorke A, Peisl J, Stangl J, Bauer G, et al. Phys Rev B 2001;63:035318. http://dx.doi.org/10.1103/PhysRevB.63.035318.

[153] Boscherini F, Capellini G, DiGaspare L, Rosei F, Motta N, Mobilio S. Appl Phys Lett 2000;76:682. http://dx.doi.org/10.1063/1.125860.

[154] Kolobov AV, Oynagi H, Wei S, Brunner K, Abstreiter G, Tanaka K. Phys Rev B 2002;66:075319. http://dx.doi.org/10.1103/PhysRevB.66.075319.

[155] Grenier S, Proietti MG, Renevier H, Gonzalez L, Garcia JM, Garcia J. Europhys Lett 2002;57:499. http://dx.doi.org/10.1209/epl/i2002-00489-5.

[156] Floro JA, Sinclair MB, Chason E, Freund LB, Twesten RD, Hwang RQ, et al. Phys Rev Lett 2000; 84:701. http://dx.doi.org/10.1103/PhysRevLett.84.70.

[157] Chason E, Sinclair MB, Floro JA, Hunter JA, Hwang RQ. Appl Phys Lett 1998;72:3276. http://dx.doi.org/10.1063/1.121622.

[158] Hulicius E, Oswald J, Pangrác J, Vyskocil J, Hospodková A, Kuldová K, et al. J Cryst Growth 2008; 310:2229. http://dx.doi.org/10.1016/j.jcrysgro.2007.11.055.

[159] Pohl UW, Pötschke K, Kaiander I, Zettler J-T, Bimberg D. J Cryst Growth 2004;272:143.

http://dx.doi.org/10.1016/j.jcrysgro.2004.08.102.
[160] Holm M, Pistol M-E, Pryor C. J Appl Phys 2002;92:932. http://dx.doi.org/10.1063/1.1486021.
[161] Kastner MA. Phys Today 1993;46:24. http://dx.doi.org/10.1063/1.881393.
[162] Woggon U. Optical properties of semiconductor quantum dots. Springer-Verlag GmbH; 1997. ISBN: 978-3540609063.
[163] Bratschitsch R, Leitenstorfer A. Nat Mater 2006;5:855. http://dx.doi.org/10.1038/nmat1768.
[164] Phillips JC, Lucovsky G. Bonds and bands in semiconductors. 2nd ed. Momentum Press; 2009. ISBN: 978-1606501337.
[165] Kroemer H. Rev Mod Phys 2001;73:783. http://dx.doi.org/10.1103/RevModPhys.73.783.
[166] Pryor CE, Pistol M-E. Phys Rev B 2005;72:205311. http://dx.doi.org/10.1103/PhysRevB.72.205311.
[167] Betcke MM, Voss H. Nanotechnology 2008;19:165204. http://dx.doi.org/10.1088/0957-4484/19/16/ 165204.
[168] Timm R, Eisele H, Lenz A, Becker SK, Grabowski J, Kim T-Y, et al. Appl Phys Lett 2004;85:5890. http://dx.doi.org/10.1063/1.1833560.
[169] Voon LY, Willatzen LC. The k p method: electronic properties of semiconductors. Morten; 2009. ISBN: 978-3540928713.
[170] [a] Grundmann M, Stier O, Bimberg D. Phys Rev B 1995;52:11969. http://dx.doi.org/10.1103/ PhysRevB.52.11969;[b] Stier O, Grundmann M, Bimberg D. Phys Rev B 1999;59:5688. http://dx.doi.org/10.1103/ PhysRevB.59.5688.
[171] Cornet C, Schliwa A, Even J, Dore F, Celebi C, Le toublon A, et al. Phys Rev B 2006;74:035312. http://dx.doi.org/10.1103/PhysRevB.74.035312.
[172] Harrison P. Quantum wells, wires and dots: theoretical and computational physics of semi- conductor nanostructures. 3rd ed. Wiley; 2009. ISBN: 978-0-470-77097-9.
[173] http://www.nextnano.com/nextnano3/ tutorial /3Dtutorial_QD_pyramid.htm.
[174] Reuter D. Capacitance-Voltage Spectroscopy of InAs Quantum Dots. In: Wang ZM, editor. Self assembled quantum dots. Springer; 2008. p. 337. ISBN: 978-0-387-74190-1.
[175] Finley JJ, Mowbray DJ, Skolnick MS, Ashmore AD, Baker C, Monty AFG, et al. Phys Rev B 2002;66: 153316. http://dx.doi.org/10.1103/PhysRevB.66.153316.
[176] Marzin J-Y, Ge rard J-M, Izrae l A, Barrier D, Bastard G. Phys Rev Lett 1994;73:716. http://dx.doi.org/10.1103/PhysRevLett.73.716.
[177] Grundmann M, Christen J, Ledentsov NN, Bo hrer J, Bimberg D, Ruvimov SS, et al. Phys Rev Lett 1995;74:4043. http://dx.doi.org/10.1103/PhysRevLett.74.4043.
[178] Maltezopoulos T, Bolz A, Meyer C, Heyn C, Hansen W, Morgenstern M, et al. Phys Rev Lett 2003; 91:196804. http://dx.doi.org/10.1103/PhysRevLett.91.196804.
[179] Vdovin EE, Khanin Yu N, Dubrovskii Yu V, Veretennikov A, Levin A, Patane A, et al. Physics- Uspekhi 2001;44:1299. http://dx.doi.org/10.1070/PU2001v044n12ABEH001055.
[180] Hayne M, Bansal B. Luminescence 2012;27:179. http://dx.doi.org/10.1002/bio.2342.
[181] Benson O, Santori C, Pelton M, Yamamoto Y. Phys Rev Lett 2000;84:2513. http://dx.doi.org/10. 1103/PhysRevLett.84.2513.
[182] Reithmaier JP, Seogonk G, Lo f?er A, Hofmann C, Kuhn S, Reitzenstein S, et al. Nature 2004; 432:197. http://dx.doi.org/10.1038/nature02969.
[183] Arakawa Y, Sakaki H. Appl Phys Lett 1982;40:939. http://dx.doi.org/10.1063/1.92959.
[184] Asada M, Miyamoto Y, Suematsu Y. IEEE J Quant Electron 1986;22:1915. http://dx.doi.org/10.1109/JQE.1986.1073149.
[185] Kirstaedter N, Ledentsov NN, Grundmann M, Bimberg D, Ustinov VM, Ruvimov SS, et al. Electron Lett 1994;30:1416. http://dx.doi.org/10.1049/el:19940939.
[186] Mi Z, Yang J, Bhattacharya P, Huffaker DL. Electron Lett 2006;42:121. http://dx.doi.org/10.1049/el:20063582.
[187] Wang T, Liu H, Lee A, Pozzi F, Seeds A. Opt Express 2011;19:11381. http://dx.doi.org/10.1364/OE.19.011381.
[188] Liu H, Wang T, Jiang Q, Hogg R, Tutu F, Pozzi F, et al. Nat Photonics 2011;5:416. http://dx.doi.org/10.1038/nphoton.2011.120.
[189] Liu GA, Stintz H, Li H, Malloy KJ, Lester LF. Electron Lett 1999;35:1163. http://dx.doi.org/10.1049/el:19990811.
[190] Zhukov AE, Kovsh AR, Maleev NA, Mikhrin SS, Ustinov VM, Tsatsulnikov AF, et al. Appl Phys Lett 1999;75:1926. http://dx.doi.org/10.1063/1.124873.
[191] Liu GT, Stintz A, Li H, Newell TC, Gray AL, Varangis PM, et al. IEEE J Quant Electron 2000;36:1272. http://dx.doi.org/10.1109/3.890268.
[192] Deppe DG, Shavritranuruk K, Ozgur G, Chen H, Freisem S. Electron Lett 2009;45:54. http://dx.doi.org/10.1049/el:20092873.
[193] Crump P, Patterson S, Elim S, Zhang S, Bougher M, Patterson J, et al. Proc SPIE 2007;6456(64560E). http://dx.doi.org/10.1117/12.706177.
[194] Kageyama T, Takada K, Nishi K, Yamaguchi M, Mochida R, Maeda Y, et al. Proc SPIE 2012; 8277(82770C). http://dx.doi.org/10.1117/12.905873.
[195] Zhukov AE, Kovsh AR, Ustinov VM, Ledentsov NN, Alferov Zh I. Microelectron Eng 2005;81:229.
[196] Seravalli L, Minelli M, Frigeri P, Franchi S, Guizzetti G, Patrini M, et al. J Appl Phys 2007;101: 024313. http://dx.doi.org/10.1063/1.2424523.
[197] Li SG, Gong Q, Cao CF, Wang XZ, Yan JY, Wang Y, et al. Infrared Phys Technol 2013;60:216. http://dx.doi.org/10.1016/j.infrared.2013.05.002.
[198] Lelarge F, Dagens B, Renaudier J, Brenot R, Accard A, van Dijk F, et al. IEEE J Sel Top Quant Electron 2007;13:113. http://dx.doi.org/10.1109/JSTQE.2006.887154.
[199] Saito H, Nishi K, Sugou S. Appl Phys Lett 2001;78:267. http://dx.doi.org/10.1063/1.1339846.
[200] Paranthoen C, Platz C, Moreau G, Bertru N, Dehaese O, Le Corre A, et al. J Cryst Growth 2003;251: 230. http://dx.doi.org/10.1016/S0022-0248(02)02473-9.
[201] Lelarge F, Rousseau B, Dagens B, Poingt F, Pommereau F, Accard A. IEEE Phot Technol Lett 2005; 17:1369. http://dx.doi.org/10.1109/LPT.2005.848279.
[202] Li SG, Gong Q, Lao YF, He K, Li J, Zhang YG, et al. Appl Phys Lett 2008;93:111109. http://dx.doi.org/10.1063/1.2985900.

[203] Kotani J, van Veldhoven PJ, No tzel R. Appl Phys Express 2010;3:072101. http://dx.doi.org/10.1143/APEX.3.072101.
[204] Qiu Y, Uhl D, Keo S. Appl Phys Lett 2004;84:263. http://dx.doi.org/10.1063/1.1640467.
[205] Tanaka S, Hirayama H, Aoyagi Y, Narukawa Y, Kawakami Y, Fujita S, et al. Appl Phys Lett 1997;71: 1299. http://dx.doi.org/10.1063/1.119877.
[206] Zhang M, Banerjee A, Lee C-S, Hinckley JM, Bhattacharya P. Appl Phys Lett 2011;98:221104. http://dx.doi.org/10.1063/1.3596436.
[207] Frost T, Banerjee A, Sun K, Chuang SL, Bhattacharya P. IEEE J Quant Electron 2013;49:923. http://dx.doi.org/10.1109/JQE.2013.2281062.
[208] Henini M, editor. Handbook of self assembled semiconductor nanostructures for novel devices in photonics and electronics. Elsevier; 2011 [chapter 19], ISBN 0080560474.
[209] Zhang ZY, Hogg RA, Lv XQ, Wang ZG. Adv Opt Photonics 2010;2:201. http://dx.doi.org/10.1364/AOP.2.000201.
[210] Li LH, Rossetti M, Fiore A, Occhi L, Velez C. Electron Lett 2005;41:41. http://dx.doi.org/10.1049/el:20056995.
[211] Lv XQ, Liu N, Jin P, Wang ZG. IEEE Phot Tech Lett 2008;20:1742. http://dx.doi.org/10.1109/LPT.2008.2004696.
[212] Chia CK, Chua SJ, Dong JR, Teo SL. Appl Phys Lett 2007;90:061101. http://dx.doi.org/10.1063/1. 2458515.
[213] Martyniuk P, Rogalski A. Prog Quantum Electron 2008;32:89. http://dx.doi.org/10.1016/j.pquantelec.2008.07.001.
[214] Levine BF. J Appl Phys 1993;74:R1. http://dx.doi.org/10.1063/1.354252.
[215] Rogalski A. J Appl Phys 2003;93:4355. http://dx.doi.org/10.1063/1.1558224.
[216] Gunapala SD, Bandara SV, Liu JK, Hill CJ, Rafol SB, Mumolo JM, et al. Infrared Syst Photoelectron Technol Proc SPIE 2004;5563:14. http://dx.doi.org/10.1117/12.560955.
[217] Berryman KW, Lyon SA, SegevM. Appl Phys Lett 1997;70:1861. http://dx.doi.org/10.1063/1.118714.
[218] Lim H, Tsao S, Zhang W, Razeghi M. Appl Phys Lett 2007;90:131112. http://dx.doi.org/10.1063/1. 2719160.
[219] Bhattacharya P, Su XH, Chakrabarti S, Ariyawansa G, Perera AGU. Appl Phys Lett 2005;86:191106. http://dx.doi.org/10.1063/1.1923766.
[220] Su XH, Yang J, Bhattacharya P, Ariyawansa G, Perera AGU. Appl Phys Lett 2006;89:031117. http://dx.doi.org/10.1063/1.2233808.
[221] Krishna S. J Phys D Appl Phys 2005;38:2142. http://dx.doi.org/10.1088/0022-3727/38/13/010.
[222] Chakrabarti S, Stiff-Roberts A, Bhattacharya P, Kennerly S. Electron Lett 2004;40:197. http://dx.doi.org/10.1049/el:20040136.
[223] Barve AV, Shah SY, Shao J, Vandervelde TE, Shenoi RV, Jang W-Y, et al. Appl Phys Lett 2008;93: 131115. http://dx.doi.org/10.1063/1.2996410.
[224] Tsao S, Lim H, Zhang W, Razeghi M. Appl Phys Lett 2007;90:201109. http://dx.doi.org/10.1063/1. 2740111.
[225] Adhikary S, Aytac Y, Meesala S, Wolde S, Unil Perera AG, Chakrabarti S. Appl Phys Lett 2012;101: 261114. http://dx.doi.org/10.1063/1.4773373.
[226] Beeler M, Trichas E, Monroy E. Semicond Sci Technol 2013;28:074022. http://dx.doi.org/10.1088/ 0268-1242/28/7/074022.
[227] Vardi A, Akopian N, Bahir G, Doyennette L, Tchernycheva M, Nevou L, et al. Appl Phys Lett 2006; 88:143101. http://dx.doi.org/10.1063/1.2186108.
[228] Yusa H, Sakaki H. Appl Phys Lett 1997;70:345. http://dx.doi.org/10.1063/1.119068.
[229] Zhuang L, Guo L, Chou SY. Appl Phys Lett 1998;72:1205. http://dx.doi.org/10.1063/1.121014.
[230] Imamura K, Sugiyama Y, Nakata Y, Muto S, Yokoyama N. Jpn J Appl Phys 1995;34:L1445. http://dx.doi.org/10.1143/JJAP.34.L1445.
[231] Finley JJ, Skalitz M, Arzberger M, Zrenner A, Bo hm G, Abstreiter G. Appl Phys Lett 1998;73:18. http://dx.doi.org/10.1063/1.122524.
[232] Wieczorek W, Warming T, Geller M, Bimberg D, Cirlin GE, Zhukov AE, et al. Appl Phys Lett 2007;88: 182107. http://dx.doi.org/10.1063/1.2200734.
[233] Marent A, Nowozin T, Geller M, Bimberg D. Semicond Sci Technol 2011;26:014026. http://dx.doi.org/10.1088/0268-1242/26/1/014026.
[234] Marent A, Geller M, Schliwa A, Feise D, Po tschke K, Bimberg D, et al. Appl Phys Lett 2007;91: 242109. http://dx.doi.org/10.1063/1.2824884.
[235] Kardynal BE, Shields AJ, OSullivan MP, Beattie NS, Farrer I, Ritchie DA, et al. Meas Sci Technol 2002;13:1721. http://dx.doi.org/10.1088/0957-0233/13/11/308.
[236] Awschalom DD, Loss D, Samarth N, editors. Semiconductor spintronics and quantum computa- tion. Springer; 2002. ISBN: 3540421769.
[237] Ludwig A, Sothmann B, Ho pfner H, Gerhardt NC, Nannen J, Ku mmell T, et al. Quantum dot spintronics: fundamentals and applications. In: Magnetic nanostructures Springer tracts in modern physics, vol. 246; 2013. p. 235. http://dx.doi.org/10.1007/978-3-642-32042-2_7
[238] Shields AJ. Nat Photonics 2007;1:215. http://dx.doi.org/10.1038/nphoton.2007.46.
[239] Rastelli A, Ulrich SM, Pavelescu E-M, Leinonen T, Pessa M, Michler P, et al. Superlattices Microstruct 2004;36:181. http://dx.doi.org/10.1016/j.spmi.2004.08.024.